Retreat and stabilization of a marine-based ice margin along a high arctic fjord-cross-shelf trough system

Pierre-Olivier Couette, Patrick Lajeunesse, Jean-François Ghienne, Boris Dorschel, Catalina Gebhardt, Dierk Hebbeln, Etienne Brouard

Retreat and stabilization of a marine-based ice margin along a High Arctic fjord-cross-shelf trough system

Pierre-Olivier Couette[1,2,*], Patrick Lajeunesse[1], Jean-François Ghienne[2], Boris Dorschel[3], Catalina Gebhardt[3], Dierk Hebbeln[4] & Etienne Brouard[5,6]

[1] *Département de Géographie, Université Laval, Québec, G1V 0A6, Canada*

[2] *Institut Terre Environnement de Strasbourg (ITES), UMR 7063, CNRS—Université de Strasbourg, France*

[3] *Alfred-Wegener-Institut Helmholtz-Zentrum für Polar- und Meeresforschung (AWI), Bremerhaven, Germany*

[4] *MARUM, Center for Marine Environmental Sciences, University of Bremen, Bremen, Germany*

[5] *Département des sciences de la Terre et de l'atmosphère & GEOTOP, Université du Québec à Montréal, H3C 3P8, Canada*

[6] *Geological Survey of Canada, Natural Resources Canada, Ottawa, Canada*

* Corresponding author

E-mail address: pierre-olivier.couette.1@ulaval.ca (P.O. Couette)

Abstract

Multibeam bathymetric and seismostratigraphic data collected in the Clyde fjord-cross-shelf trough system (eastern Baffin Island, Canadian Arctic Archipelago) display glacial landforms and depositional assemblages that enable the identification of the maximal extent of the Laurentide Ice Sheet (LIS) margin and delineating the patterns and controls on its subsequent retreat. Additionally, 10 new sediment cores – from which seven radiocarbon ages were acquired – allow the recognition of depositional processes. Results show that, during the Last Glacial Maximum, the LIS margin extended almost to the edge of the continental shelf. Early deglaciation of the trough was marked by an initial ice-shelf collapse and rapid retreat of the ice stream, as evidenced by the absence of ice marginal landforms and the presence of extensive iceberg ploughmarks across a large portion of the outer trough. It was followed by a slow retreat and successive stabilizations of the ice margin that led to the deposition of recessional moraines and GZWs. Deglaciation of the fjord in the early Holocene occurred in an episodic style, whereby rapid retreat was punctuated by relatively long standstills that enabled major moraine formation. Long-term stabilizations of the ice margin in the Clyde fjord-cross-shelf trough system are interpreted to coincide with major climatic cooling events, such as the Younger Dryas and early Holocene cold reversals. Ages derived from sediment cores and previous work suggest that higher retreat rates correspond with periods of significant global sea level rise, suggesting that oceanic forcing exerted a minor control on the deglaciation. GZWs and large moraine ridges are observed at pinning points in the trough, indicating that the location of ice margin stabilizations was influenced by topography. The reconstruction of the deglaciation of the Clyde fjord-cross-shelf trough system allows us to refine deglacial models for similar systems of northeastern Baffin Island, in particular beyond the coast and along the steeper section of the fjord where chronological gaps remained.

Keywords: Laurentide Ice Sheet; Baffin Island; Deglaciation; Holocene; Submarine landforms; Marine sediment cores; Abrupt climatic events

1. Introduction

Reconstructing the history of past ice sheets allows to document their inter-relationship with the climate system, especially by providing boundary conditions to test models that aim to simulate climate and ice sheet evolution (Joughin et al., 2012; Stocker et al., 2013; Rasmussen et al., 2014; Tinto et al., 2019; Briner et al., 2020; Lowry et al., 2020). Past marine-based ice sheet margins such as those of the Laurentide Ice Sheet (LIS), which was in contact with the western Atlantic Ocean during the Last Glacial Maximum (LGM; ~24 ka BP), are believed to have operated in a comparable way to the present Antarctic Ice Sheet, with a network of ice streams channeled in bathymetric troughs and mass loss dominated by calving (Ottesen et al., 2005; De Angelis and Kleman, 2007; Margold et al., 2018). Reconstructing palaeo-ice sheet dynamics and deglaciation patterns is therefore fundamental for understanding the long-term behaviour of modern ice sheets (i.e., Antarctica and Greenland) and their interconnection with global climate (i.e., Danielson and Bart, 2019; Smith et al., 2019; Briner et al., 2020; Young et al., 2020, 2021).

Controls and ice-retreat patterns during the deglaciation that followed the LGM still remain poorly documented in the eastern Canadian Arctic Archipelago (CAA) compared to other deglaciated regions of the Northern Hemisphere, such as Norway (e.g., Lyså and Vorren, 1997; Aarseth et al., 2007; Laberg et al., 2009; Bjarnadóttir et al., 2012), Svalbard (e.g., Winsborrow et al., 2010; Streuff et al., 2018; Flink and Noormets, 2018; Howe et al., 2019; Allaart et al., 2020) and the British Isles (e.g., Arosio et al., 2018; Callard et al., 2020). Off Baffin Island, marine geophysical data suggest that ice retreat was punctuated by successive stabilizations of the late glacial ice margin on the continental shelf (Brouard and Lajeunesse, 2017), while onshore data suggest a rapid ice decay into the fjords during the early Holocene (Miller et al., 2005; Briner et al., 2005,

2007, 2009a; Young et al., 2015; Margreth et al., 2017). However, recent offshore investigations show that multiple ice-margin stabilizations occurred within the fjords of northeastern Baffin Island during the last deglaciation (Brouard and Lajeunesse, 2019a). Stabilizations both on the shelf and in the fjords of northeastern Baffin Island were found to be strongly influenced by bed geometry (Brouard and Lajeunesse, 2017, 2019a), similarly to observations made in other deglaciated fjords and continental shelves (i.e., Aarseth et al., 1997; Hodgson et al., 2014; Batchelor et al., 2019a). These contrasting patterns of ice retreat, which probably arise from the scarcity of valuable data from the submarine domain, complicate the establishment of a reliable model of deglaciation and outline the need for improved understanding of LIS extent and retreat patterns in the fjord-cross-shelf trough systems of Baffin Island by bridging submarine and continental data.

Here we map and analyse submarine landforms and sediment assemblages in the 180 km-long Clyde fjord-cross-shelf trough system, with the aim of refining our understanding of the retreat patterns of the marine-based margin of the northeastern LIS. By using a combination of multibeam bathymetric data, acoustic and seismic profiles as well as sediment cores, the key objectives are to 1) define a chronology for the deglaciation of the LIS in the region; 2) reconstruct changes in the morpho-sedimentary system and dynamics on the shelf and in the fjord; and 3) identify the factors that controlled ice margin retreat rates and stabilization during deglaciation.

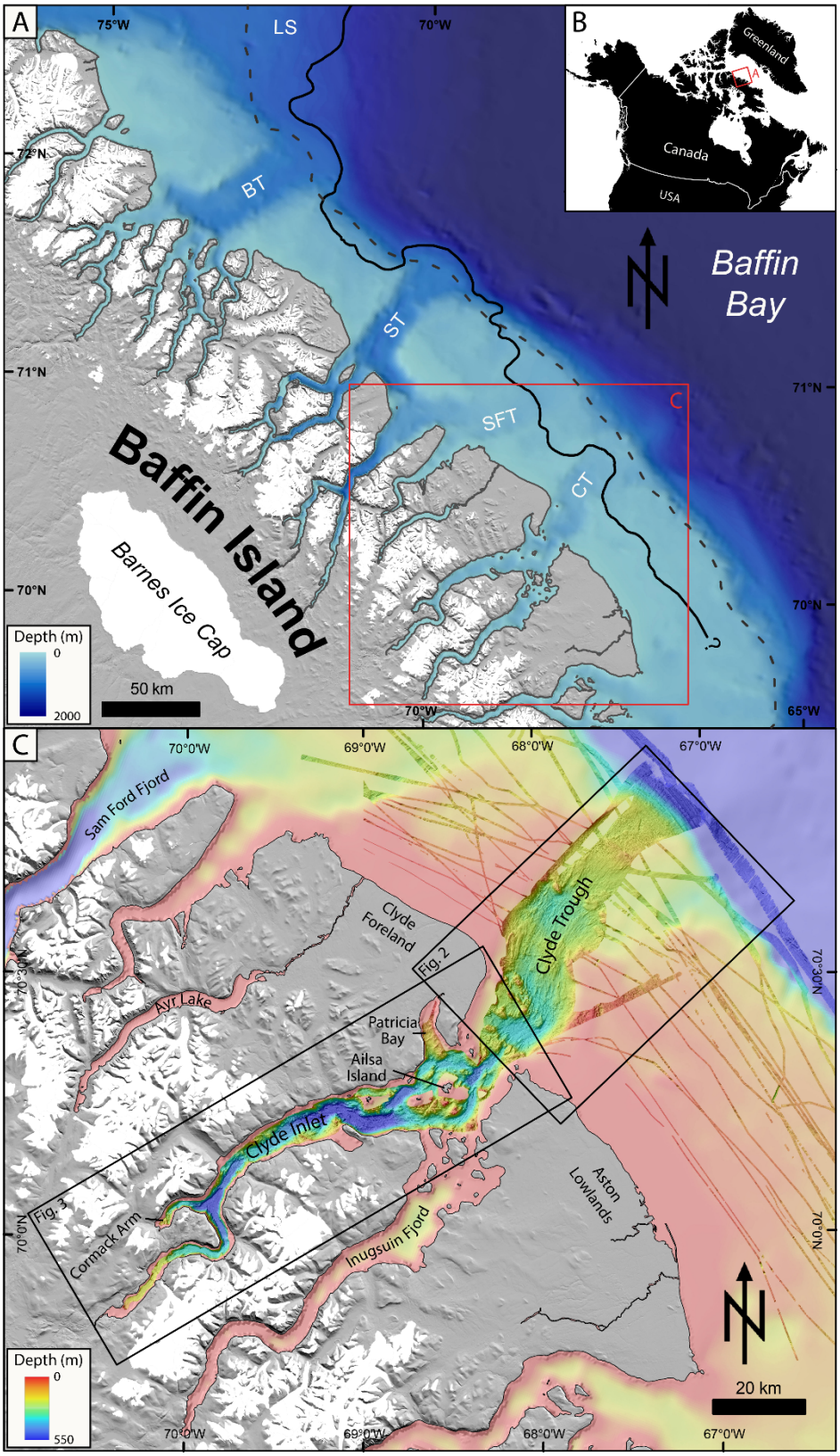

Figure 1 (A) Baffin Bay and the proposed LGM limit on northeastern Baffin Island, modified from Brouard and Lajeunesse, 2017. LS: Lancaster Sound; BT: Buchan Trough; ST: Scott Trough; SFT: Sam Ford Trough; CT: Clyde Trough. The dashed line represents the LIS extent at the LGM from Dalton et al., 2020. (B) Location of the study area. (C) Map showing the multibeam bathymetric data used in this study draped on the International Bathymetric Chart of the Arctic Ocean data gridded at a 500 m cell-size resolution (IBCAO; Jakobsson et al., 2014). The hillshade is from the Canadian Digital Elevation model (CDEM).

2. Regional setting

2.1. Study area

The studied area comprises the fjord of Clyde Inlet and its offshore extension across the continental shelf, namely Clyde Trough (Fig. 1). This fjord-cross-shelf trough system stretches from the interior plateau of Baffin Island to the shelf break facing Baffin Bay.

The continental shelf off Clyde Inlet is generally shallow (< 200 m) with a deeper trough carved by repeated occupation by ice streams during Quaternary glaciations (Løken and Hodgson, 1971; Praeg et al., 2007). Precambrian crystalline rocks extend halfway across the continental shelf, where they are overlain by upper Cretaceous-Tertiary strata of the Baffin Bay Basin (Jackson et al., 1984; Fader et al., 1989; Praeg et al., 2007). Clyde Trough is 20 to 30 km-wide, extends from SW to NE, on >60 km, and bends slightly toward the east near the shelf break. Existing coarse resolution bathymetry data (GEBCO) show that the trough is flat-bottomed and has a reverse-gradient slope (Fig. 1C), characteristic of troughs in formerly glaciated areas (Ottesen et al., 2007; Slabon et al., 2016; Arndt et al., 2017; Bart et al., 2017; Brouard and Lajeunesse, 2017), with water depths decreasing seaward from ~375 m at the mouth of the fjord to ~150 m at the shelf break.

Clyde Inlet is a fjord that has been glacially incised into the Precambrian crystalline rocks of the eastern coastal mountains of Baffin Island during Quaternary glaciations (Jackson et al., 1984; Kessler et al., 2008). With its U-shaped profile and a succession of deep basins separated by intervening sills, it has a typical mid- and high-latitude fjord morphology (Syvitski and Shaw, 1995). Clyde Inlet is 120 km-long, between 3 and 20 km-wide and consist of basins between 200 and 500 m-deep (Fig. 1C). Many hanging valleys of various widths and depths drain into Clyde Inlet, providing

125 localized sediment input through proglacial rivers. Inugsuin Fjord, a 100 km-long fjord,
126 and Patricia Bay also merge into Clyde Inlet near its mouth. Clyde Inlet is directly
127 connected to the cross-shelf trough, forming a 180 km-long submarine glacial valley
128 system connecting Baffin Island to Baffin Bay and separated by a shallow bedrock sill at
129 the fjord mouth.

130 Most of the valleys, lowlands, fjords and trough of Clyde Inlet and nearby areas
131 are covered by a thick sequence of Quaternary deposits (Jackson et al., 1984; Praeg et al.,
132 2007; Brouard and Lajeunesse, 2017, 2019a, 2019b).

133 **2.2. Late Quaternary glacial history**

134 Late Wisconsinan (MIS 2) ice sheets started building up at ~28 ka BP (Stokes et
135 al., 2012; Klassen et al., 2010; Batchelor et al., 2019b) and reached their maximal extent
136 by 24 ka BP in many sectors of North America (Dyke, 2002; Andrews and Dyke, 2007;
137 Hughes et al., 2013). Although many models have been proposed for establishing the
138 maximal extent of the LIS at the LGM, recent studies indicate that the ice margin
139 extended at or near the edge of the northeastern Baffin Island shelf (Briner et al., 2006;
140 Li et al., 2011; Brouard and Lajeunesse, 2017; Jenner et al., 2018; Dalton et al., 2020;
141 Lévesque et al., 2020; Couette et al., 2022). In between the fjords, cosmogenic exposure
142 ages on glacial erratics and bedrock suggest an extensive LIS cover during the LGM
143 (Briner et al., 2005; Davis et al., 2006). Marine geophysical data also show that an ice
144 shelf covered northern Baffin Bay during the LGM, possibly buttressing peripheral ice
145 streams and impacting their flow to the ocean (Couette et al., 2022).

146 Following the LGM, the break up of the Baffin Bay ice shelf between 16 and 14.6
147 ka BP provoked a major reorganization of the ice-sheet drainage system by removing the
148 buttressing effect on ice streams (Couette et al., 2022), and therefore led to ice-flow
149 acceleration in systems from northeastern Baffin Island (Jenner et al., 2018). This event

was found to be more or less coeval with the deposition of a detrital carbonate sediment layer in Baffin Bay (BBDC-1), corresponding to massive ice discharge from ice streams of the CAA and northwest Greenland and characterized by Ca-rich sediments (Hiscott et al., 1989; Andrews et al., 1998; Simon et al., 2014; Jackson et al., 2017; Jenner et al., 2018). This iceberg discharge event was followed by a period of important ice retreat on the shelf off eastern Baffin Island coinciding with the Bølling-Allerød warm period (Dyke et al., 2002; Briner et al., 2005; Margreth et al., 2017; Brouard and Lajeunesse, 2017; Jenner et al., 2018). The subsequent retreat towards Baffin Island mainland was punctuated by glacier readvances or stabilizations during the cold phase of the Younger Dryas (12.9-11.7 ka BP) which led to the building of major moraine systems (Briner et al., 2007; Margreth et al., 2017; Young et al., 2020). Following the Younger Dryas, and under the warmer climate of the early Holocene period, the ice margin retreated rapidly to reach the inner fjord (Andrews and Ives, 1978; Briner et al., 2007, 2009b). This rapid ice-margin retreat was temporarily interrupted by ice-margin stabilizations during short cold events at 10.3, 9.3 and 8.2 ka (Briner et al., 2007, 2009b; Young et al., 2012, 2020; Crump et al., 2020). The latter event is recorded at the fjord heads on eastern Baffin Island and referred to as the Cockburn stage moraine (Andrews and Ives, 1978; Briner et al., 2007, 2009b; Brouard and Lajeunesse, 2019a; Young et al., 2021). Subsequently, the LIS margin retreated steadily from the fjord head and separated to form what are today's Barnes and Penny ice caps (Dyke, 2004; Miller et al., 2005; Briner et al., 2009b).

3. Material and methods

This study is based on multibeam bathymetric data, shallow acoustic data, seismic data, and sediment core data. The main bathymetric dataset was acquired during expedition MSM66 of the German research vessel RV Maria S. Merian in August 2017 (Dorschel et al., 2017). The MSM66 data are complemented by bathymetric data collected

during ArcticNet cruises onboard the CCGS Amundsen (2003-2017). Shallow acoustic data and sediment cores were also collected during MSM66 (Dorschel et al., 2017). Seismic data were acquired by the Geological Survey of Canada during airgun surveys in 1978 and 1980.

3.1. Multibeam bathymetric data

MSM66 bathymetric data were collected with a Kongsberg Simrad EM122 (12 kHz) multibeam echosounder (MBES), while the CCGS Amundsen data were collected with a Kongsberg Simrad EM302 (30 kHz) MBES. These datasets were processed for anomalous data points and artefacts removal using Caris Hips and Sips software. The datasets were gridded with a 10 m cell-size resolution and then imported into ESRI ArcGIS 10.8 software for geomorphological mapping and interpretation.

3.2. Shallow acoustic and seismic data

Shallow acoustic data were recorded with an Atlas Parasound DS P-70 system (5-33 kHz) during MSM66. The raw data were recorded into PS3 format and then converted into SEGY using ps32segy software of Dr. Hanno Keil (University of Bremen). The acoustic profiles were then imported into the *SMT Kingdom Suite* software for processing and interpretation.

Seismic lines 78029_AG_275_0130 and 80028_AG_RAYT_257_0200 were acquired on expeditions 78029 (1978) and 80028 (1980) by Brian MacLean of the Geological Survey of Canada-Atlantic (Cruise reports available via https://ed.marine-geo.canada.ca/cruise_report_e.php). Extraction and interpretation was performed using the *LizardTech GeoViewer* software. Both acoustic and seismic data were transferred into Adobe Illustrator for figure production. Thicknesses and water depth were calculated using a velocity of 1500 m/s.

3.3. Core data

The sediment cores collected during expedition MSM66 were between 137 and 965 cm long (Table 1). On board, all cores were split, visually described with a particular focus on noting the lithology, texture, contacts, sedimentary structures and Munsell colour, as well as digitally photographed.

Table 1 Information on cores collected in the Clyde fjord-cross-shelf trough system.

Core name	Latitude	Longitude	Water depth (m)	Core length (cm)
GeoB22344-3	70°03.90'N	70°02.93'W	367	483
GeoB22346-3	69°54.18'N	70°13.54'W	203	783
GeoB22348-3	69°58.47'N	69°57.47'W	362	896
GeoB22350-3	70°08.52'N	69°44.36'W	435	137
GeoB22351-3	70°10.16'N	69°38.30'W	364	523
GeoB22353-3	70°13.35'N	69°00.16'W	489	862
GeoB22356-3	70°27.68'N	67°58.36'W	338	965
GeoB22357-3	70°36.28'N	67°53.63'W	315	902
GeoB22358-3	70°41.69'N	67°41.83'W	261	500
GeoB22359-3	70°46.06'N	67°27.96'W	196	166

X-ray fluorescence (XRF) scanning were used to characterize elemental properties of the sediments by using a XRF Core Scanner II (AVAATECH Serial No. 2) at MARUM, University of Bremen. Data were collected every 2 cm down-core over a 15 mm^2 area with down-core slit size of 10 mm using generator settings of 10 kV, a current of 0.2 mA and a sampling time of 10 seconds directly at the split core surface of the archive half. The split core surface was covered with a 4 µm thin SPEXCerti Prep Ultralene1 foil to avoid contamination of the XRF measurement unit and desiccation of the sediment. Raw spectra data were processed by the analysis of X-ray spectra in the Iterative Least square software (WIN AXIL) package from Canberra Eurisys.

Accelerator Mass Spectrometry (AMS) radiocarbon dating was carried out on benthic foraminifera assemblages and shell fragments. Samples were sent to the MICADAS-laboratory (Alfred Wegener Institute, Bremerhaven), where CO_2 from small amount of foraminiferal carbonate (~0.5mg) were analysed. Additionally, three dates

based on shell fragments were obtained. The AMS ^{14}C ages were converted to calendar years before present (cal. BP) using the online software Calib 8.2 with the Marine20 radiocarbon age calibration curve (Heaton et al., 2020). The Marine20 calibration curve uses a global marine reservoir age that is not suitable for the polar regions, an issue that requires the application of additional reservoir correction (ΔR) values to high-latitudes samples (Heaton et al., 2020). Therefore, an additionnal local ΔR of 81 ± 18 was used to account for the regional offset of the world ocean ^{14}C age (Pieńkowski et al., 2022). The ΔR value is kept constant for the entire period, although we acknowledge that oceanographic conditions such as circulation, ventilation and extensive sea-ice cover during glacial periods may result in the overestimation of the actual calendar ages (Heaton et al., 2022; Pieńkowski et al., 2022). However, as our ages are from the early Holocene, they were likely little affected by such changes in oceanographic conditions. We argue that using only an additional local reservoir correction therefore provides an appropriate estimate for these ages, with relatively minimal uncertainties.

4. Results

4.1. Seafloor geomorphology

Complete multibeam bathymetric coverage of the Clyde fjord-cross-shelf trough system allowed identifying several submarine glacial landforms (Fig. 2 and 3) that are here described and interpreted for reconstructing the past configuration, stages and dynamics of the LIS margin.

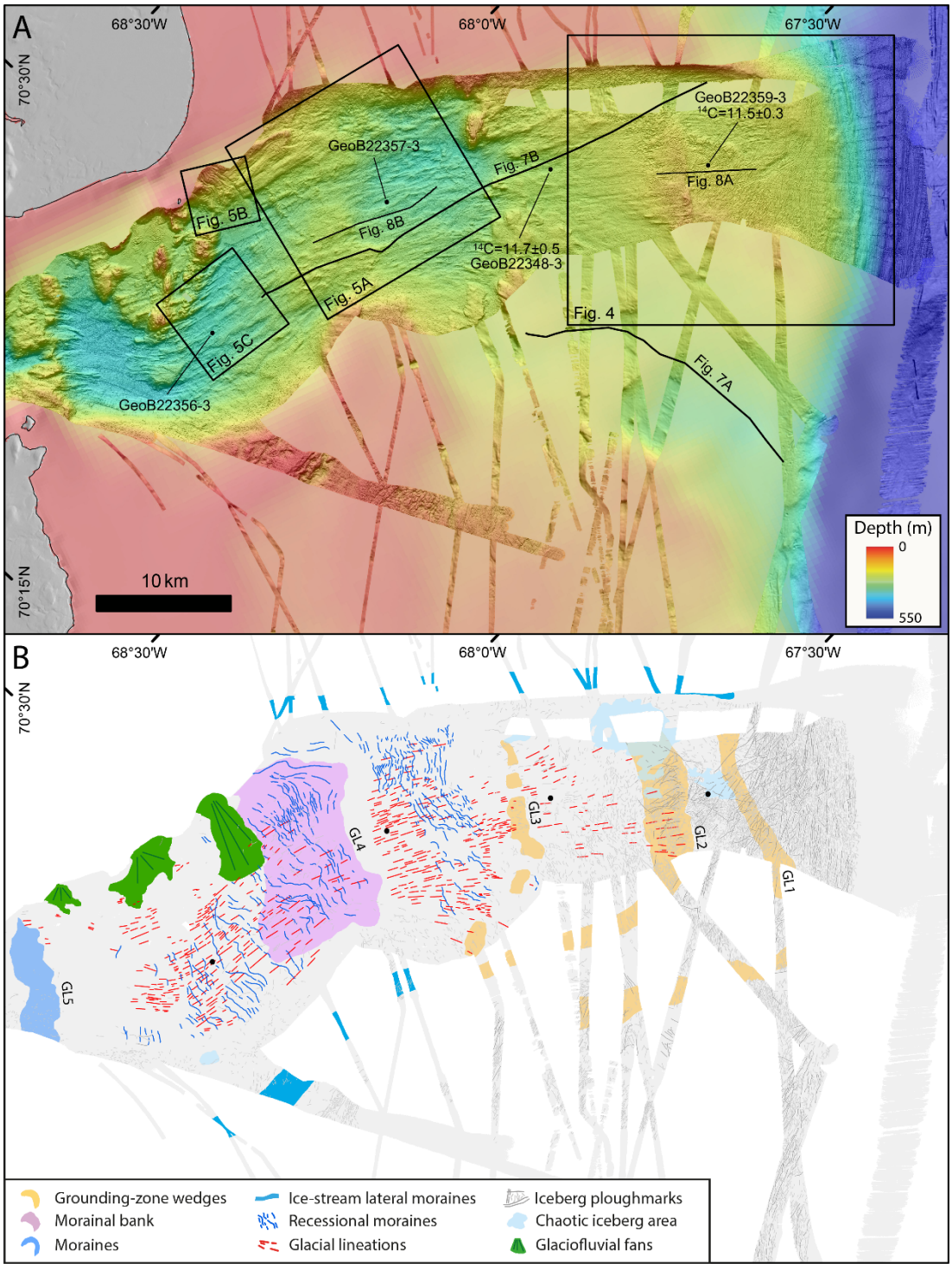

Figure 2 (A) Multibeam bathymetry of Clyde Trough. Boxes show the location of Figs. 4 and 5. Dashed brown lines represent moraine ridges from Briner et al. (2007). Ages derived from the sediment cores represent minimum age for deglaciation at the core site. (B) The mapped distribution of submarine landforms in the trough.

4.1.1. Subglacial landforms

Several streamlined landforms oriented along the fjord and trough axis occur in the Clyde fjord-cross-shelf trough system and represent variations in ice-flow direction and velocity. They are here grouped under the generic term glacial lineations.

Glacial lineations - Sets of streamlined and curvilinear ridges oriented parallel to the trough axis are observed at depths between 100 m and 500 m; they are up to 5 km-long (Fig. 4, 5A, 5C, 6A and 6D). These streamlined landforms are between 50 m to 500 m-wide and can be as much as 60 m-high compared to the surrounding seafloor. These ridges are mostly aligned parallel to each others, but are in some cases divergent where the trough widens. Features with lower length to width ratios (between 1:5 and 1:20) tend to be asymmetrical, with a gentler seaward slope, and occur mostly beyond bedrock outcrops. Conversely, ridges with higher length to width ratios (up to 1:50) are more symmetrical, subtle and tend to have a smoother appearence. These ridges are in some cases superimposed on grounding line landforms.

These streamlined landforms are interpreted as glacial lineations, such as mega-scale glacial lineations (MSGLs), drumlins and crag-and-tails, which provide evidence for former ice-flow directions as they are parallel to another (Clark, 1993; Stokes and Clark, 2001; Spagnolo et al., 2014; Dowdeswell et al., 2016; Maclean et al., 2016; Batchelor et al., 2018; Ottesen et al., 2022). Glacial lineations are differentiated on the basis of their width to length ratio and their formation processes. MSGLs are generally highly elongated (up to 1:50 length to width ratio) and are produced by the deformation of soft till beneath a fast-flowing ice stream (e.g., Clark, 1993) or as a product of ice keels ploughing through sediments (e.g., Tulaczyk et al., 2001; Clark et al., 2003). In turn, crag-and-tails and drumlins are less elongated (between 1:5 and 1:20 length to width ratio) and formed by the accumulation of sediments on the seaward side of bedrock obstacles or the streamlining of bedrock by ice (Stokes and Clark, 2001; Ottesen et al., 2007). The position of most crag-and-tails beyond bedrock in Clyde Inlet suggests that they were formed by the streamlining action of warm-based ice (Dowdeswell et al., 2016; Maclean et al., 2016).

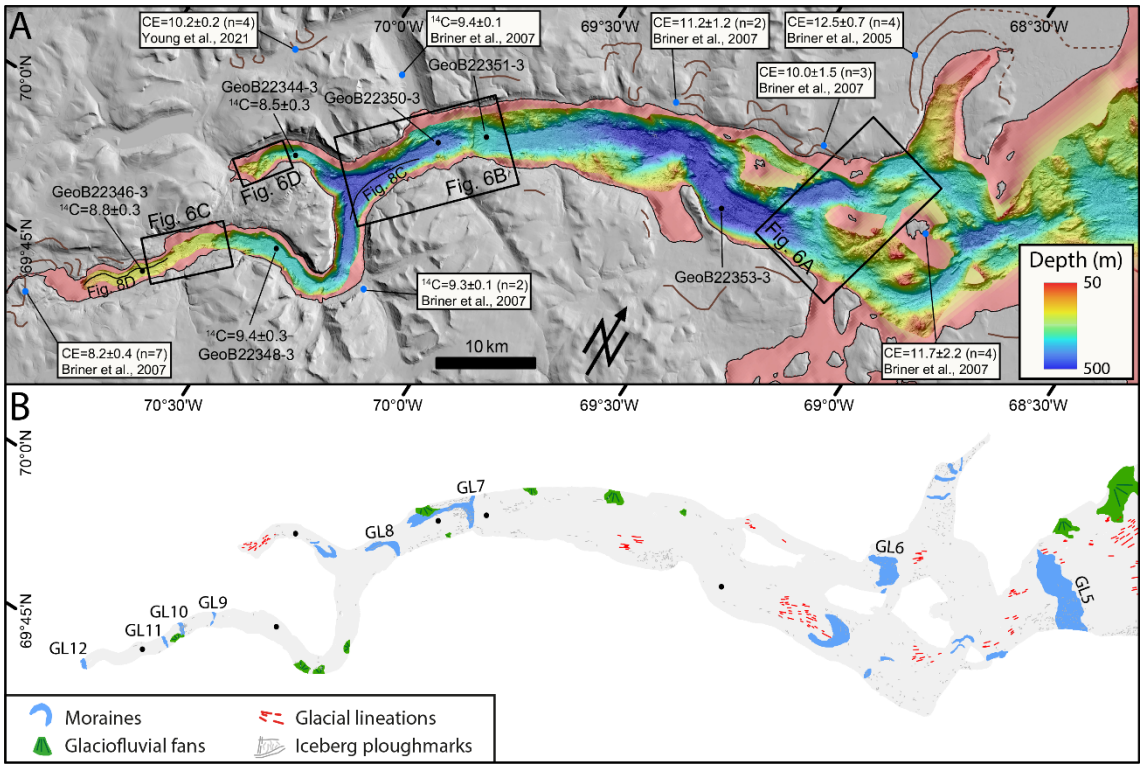

Figure 3 (A) Bathymetry of Clyde Inlet. Boxes show the location of Fig. 6A-D. Brown lines represent moraine ridges from Briner et al. (2007). Ages derived from the sediment cores represent minimum age for deglaciation at the core site. Blue dots indicate cosmogenic exposure (CE) and radiocarbon (^{14}C) dating discussed in the text, compiled from previous studies along Clyde Inlet (in ka ± 1 SD uncertainties). (B) The mapped distribution of submarine landforms in the fjord.

4.1.2. Ice marginal landforms

Several sediment wedges and ridges are observed on the multibeam bathymetry imagery and record the extent and retreat pattern of the LIS during the LGM and the deglaciation. GZWs, morainal bank, and end moraines represent major grounding line landforms (refered to as GL in Figs. 2-3 and in the discussion) that record former, successive position of the ice margin along the Clyde fjord-cross-shelf trough system.

Grounding-zone wedges (GZWs) - Asymmetric transverse wedges characterized by steeper ice-distal slope are identified in the outer and middle part of Clyde Trough (Fig. 4 and 7). These wedges are present at water depths ranging from 150 m to 350 m, have lengths between 3 and 10 km and rise from 20 to 50 m above the surrounding seafloor. On the seismic data, they correspond to wedge-like deposits reaching 15 to 20 m in thickness and 5 km in length (Fig. 7) with low-reflectivity, transparent and

sometimes chaotic acoustic signature. Smooth and gently sloping fan-shaped surfaces (between 0.5 and 2°) are usually identified on the seafloor in front of those large transverse wedges.

Due to their asymmetric geometry and steep ice-distal slopes, these asymmetric wedges are interpreted as grounding-zone wedges similar to ice-contact wedges reported on other deglaciated continental shelves (e.g., Ottesen et al., 2007, 2022; Slabon et al., 2016; Brouard and Lajeunesse, 2017). Large GZWs are formed during relatively long-term ice margin stabilizations (decadal- to centennial-scale) which enable subglacial sediment accumulation at the grounding line (Powell and Domack, 1995; Dowdeswell and Fugelli, 2012; Batchelor and Dowdeswell, 2015). The accumulation of sediment is interpreted to be vertically limited by the presence of a floating ice shelf seaward from the grounded ice, thus favoring horizontal progradation of sediments and forming low-amplitude extensive wedges (Dowdeswell and Fugelli, 2012 ; Batchelor and Dowdeswell, 2015). The fan-shaped surfaces are interpreted as ice-marginal debris flow lobes deposited by sediment delivery at the grounding line of a marine terminating glacier (Syvitski and Shaw, 1995; Ó Cofaigh and Dowdeswell, 2001; Bjarnadóttir et al., 2012; Batchelor and Dowdeswell, 2015; Dowdeswell et al., 2015; Ottesen et al., 2017).

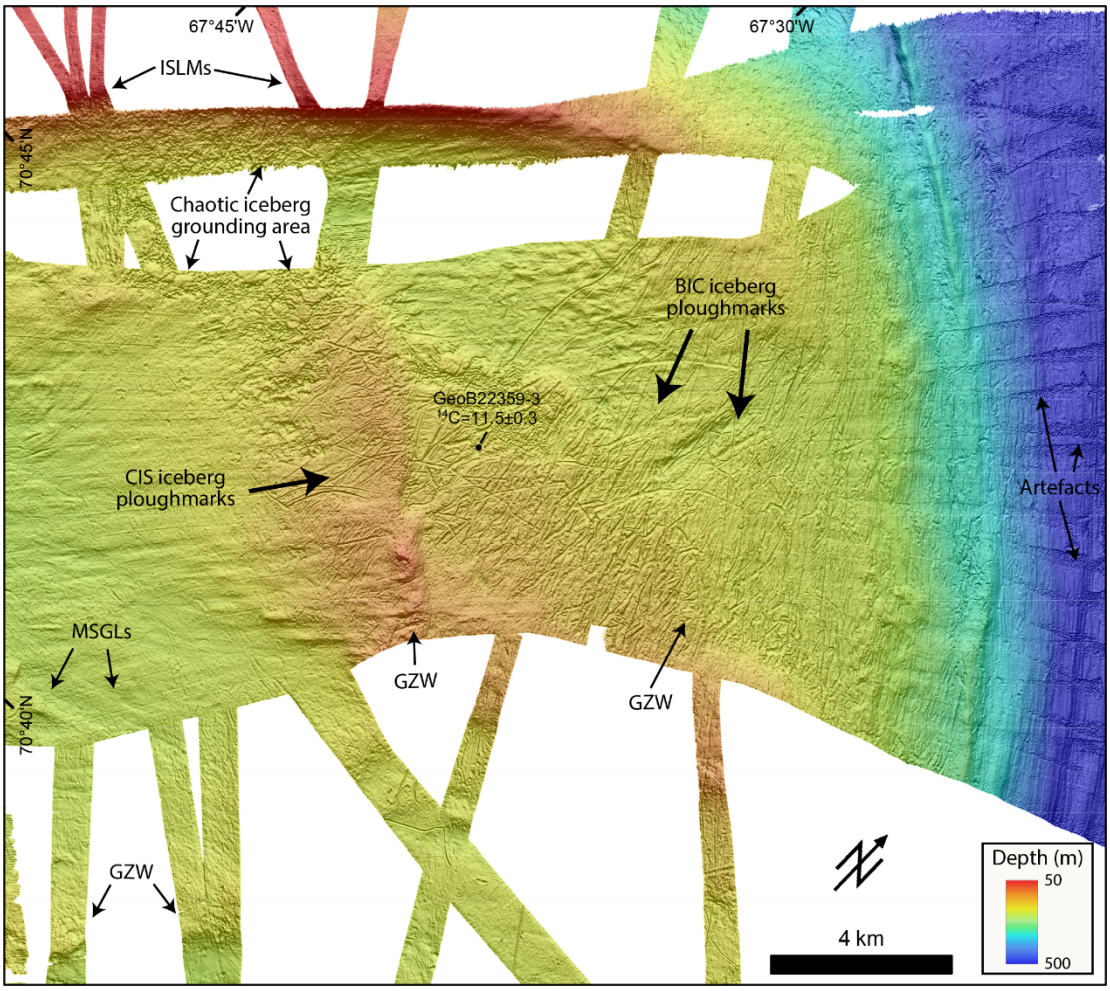

Figure 4 Multibeam bathymetry of submarine landforms in the outer trough. CIS – Clyde Ice Stream and BIC – Baffin Island Current. For further interpretation and discussion, see Couette et al. (2022).

Morainal banks – A large asymmetric wedge with a steeper ice-distal side and overprinted by transverse zigzag-shaped ridges and recessional moraines is located in the center of Clyde Trough at a depth of 325 m (Fig. 5A and 7B). The wedge is 75 m-high, 6 km-long and 12 km-wide, while the overprinting zigzag-shaped ridges are 5-10 m-high, 100 to 200 m-long and between 500 and 1000 m-wide (Fig. 5A). The seismic data show three distinct morpho-sedimentary units composing the underlying sediment body: (1) a bottom unit showing evidence of glaciotectonism including folds and thrust sheets; (2) an upper unit showing seaward dipping reflectors; and 3) ridges with a chaotic acoustic signature located on the stoss side of the system. Gently sloping fan-shaped surfaces are identified in front of this large asymmetric wedge. The associated deposits attenuate underlying landforms such as glacial lineations and recessional moraines (Fig. 5A).

Based on its morphology and the overprinted zigzag-shaped ridges, this landform is interpreted as a morainal bank. Morainal banks are generally associated with a quasi-stagnant ice margin position during overall deglaciation, coherent with the presence of recessional moraines (Powell, 1981; Christofferson and Tulaczyk, 2003; Laberg et al., 2009; Dowdeswell et al., 2015). Zigzag-shaped ridges are, in turn, associated with sediment deformation related to push and thrust of ice proximal deposits by glacier readvances (Powell, 1981; Christofferson and Tulaczyk, 2003; Laberg et al., 2009). They could also represent crevasse-squeeze ridges, produced subglacially by basal till being squeezed into crevasses at the glacier bed during an ice advance (Evan and Rea, 1999; Ottesen et al., 2022). The complex acoustic signature with folds and thrust sheets observed on the seismic profile (Fig. 7B) further support the interpretation of a readvance of the ice margin that lead to the formation of the morainal bank (Laberg et al., 2009). The fan-shaped surfaces observed in front of the morainal bank are interpreted as ice-marginal debris flow lobes (Syvitski and Shaw, 1995; Ottesen et al., 2017).

Major end moraines - Arcuate asymmetrical ridges with a steeper ice-proximal slope are observed at several locations along Clyde Inlet (Figs. 6B-C). These landforms range between 10 m and 150 m in height, and between 1 km and 6 km in width. They are 500 m to 3 km-long and are observed at depths reaching 450 m. On the distal flank, fan-shaped surfaces occasionally emanate from the ridges over distances of several kilometers. Ridges located in Patricia Bay have a more subtle and smoother appearance (Fig. 3). Partially buried transverse ridges with steep-scarps are also observed at a few locations in the fjord, where they bound step-like basins (Figs. 6B-C). Several linear ridges running parallel to the fjord axis and specifically located on the flanks of the fjord are also observed in Clyde Inlet (Fig. 6B). These ridges are 500 m to 3 km-long, 100 m

346 to 500 m-wide, up to 100 m-high and appear to be, in some cases, the lateral extension of
347 the arcuate ridges (Figs. 5A and 6B).

348 Due to their geometry and their position transverse to the fjord axis, the arcuate
349 ridges are interpreted as major end moraines, whereas the linear and parallel-to-the-fjord
350 morphologies are, in turn, interpreted as lateral moraines (Dowdeswell and Vásquez,
351 2013; Dowdeswell et al., 2014; Hodgson et al., 2014). Major end moraines are formed by
352 the deposition and pushing of sediment during long-term ice margin stabilizations of at
353 least decades to centuries (Powell and Alley, 1997; Dowdeswell et al., 2014; Batchelor et
354 al., 2018). In contrast to GZWs, moraine ridges usually develop at the margin of tidewater
355 glacier that are vertically unrestricted accommodation space at the grounding line (Powell
356 and Alley, 1997). Similarly to observations in front of GZWs and the morainal bank, the
357 fan-shaped surfaces are inferred to be ice-marginal debris flow lobes (Syvitski and Shaw,
358 1995; Ottesen et al., 2017). The moraine ridges in Patricia Bay probably represent
359 deposition by a secondary ice flow across the bay and onto the Clyde forelands (Briner et
360 al., 2005). The step-like basins observed in the fjord are interpreted to be the result of
361 high sediment deposition from transverse deltas fed by nearby rivers and overfilling some
362 of the basins confined by a succession of receding moraines (Hodgson et al., 2014;
363 Brouard and Lajeunesse, 2019a).

364 *Recessionnal moraines* - Small ridges transverse to the former ice flow are
365 specifically identified on the multibeam bathymetric data of the trough (Fig. 5A). They
366 are observed in the mid- to inner section of the trough in water depths ranging from 200
367 m to 300 m; their size varies between 2 m and 12 m-high and 100 m to 500 m-wide. Some
368 of them can be traced for lengths of >5 km, although the majority do not exceed 1 km.
369 Most of the ridges are arcuate and symmetric. They occur in two distinct clusters of
370 parallel to sub-parallel features spaced a few hundred meters apart.

These small parallel ridges are interpreted as recessional moraines, formed by the delivery and pushing of subglacial sediments by minor stillstands or readvances of the grounded glacier front in subaqueous conditions (Boulton, 1986; Lindén and Möller, 2005; Dowdeswell et al., 2008; Ó Cofaigh et al., 2008; Arndt et al., 2017; Batchelor et al., 2018; Howe et al., 2019; Ottesen et al., 2022). The presence of recessional moraines in marine environments is usually associated with a relatively slow retreat of the ice margin in water typically shallower than 350 m (Lindén and Möller, 2005; Dowdeswell et al., 2008; Ó Cofaigh et al., 2008; Howe et al., 2019).

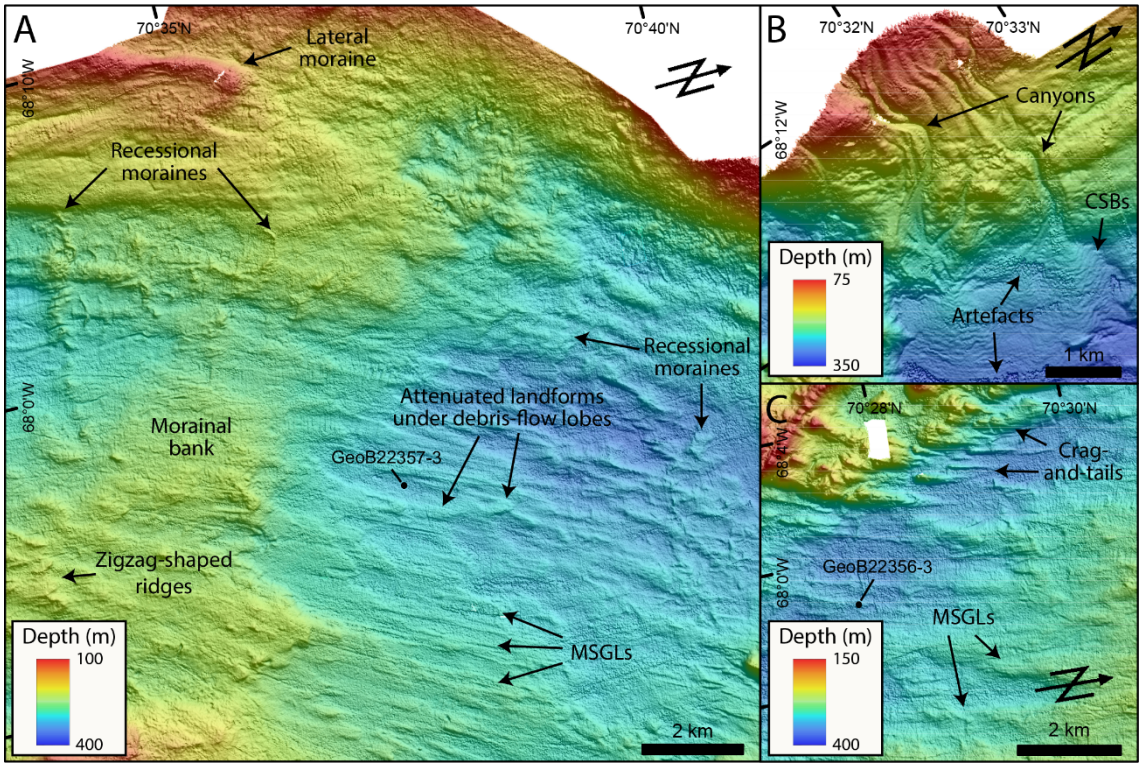

Figure 5 (A) Multibeam bathymetry of submarine landforms in the middle trough. (B) Example of a glaciofluvial fan, with associated canyons and CSBs, in the middle trough. (C) Example of mega-scale glacial lineations (MSGLs) in the inner trough.

Ice stream lateral moraines - Elongated ridges orientated parallel to the former ice flow are observed at the lateral boundaries of Clyde Trough (Fig. 4). They are up to 25 m-high, 1 to 3 km-wide and occur at depths between 50 m to 175 m. These ridges have a steeper trough-proximal slope and are observed on both sides of the trough.

These extensive elongated ridges are interpreted as ice-stream lateral moraines based on their shape, dimensions and location at the margins of the trough (Ottesen et al., 2007; Rydningen et al., 2013; Batchelor and Dowdeswell, 2016; Brouard and Lajeunesse, 2019b). They have been suggested to be formed mainly from the accumulation of subglacial till at the shear zone between fast-flowing ice stream and slow-flowing portions of an ice sheet or ice free terrain (Dyke and Morris, 1988; Stokes and Clark, 1999, 2002; Batchelor and Dowdeswell, 2016).

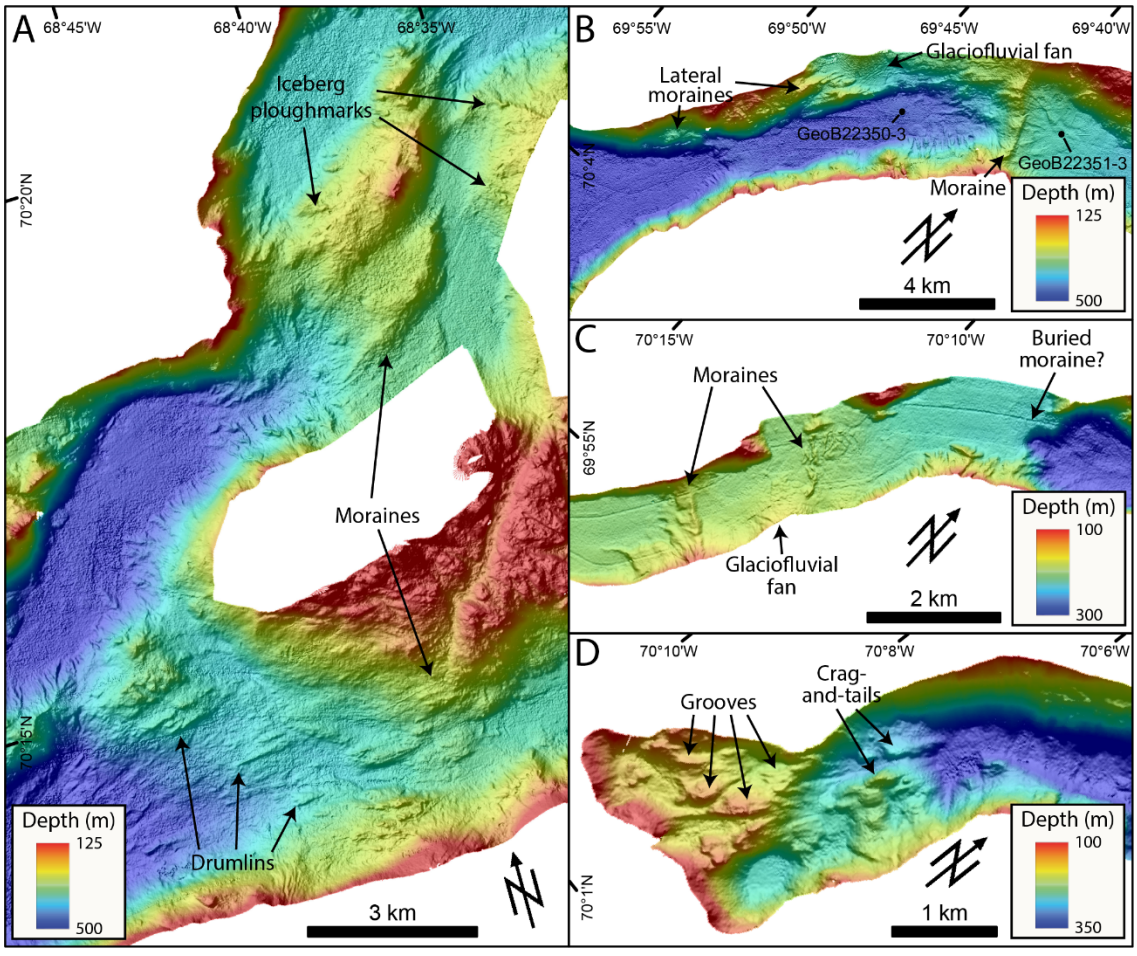

Figure 6 (A) Multibeam bathymetry of submarine landforms in the outer fjord. (B) Multibeam bathymetry of submarine landforms in the middle fjord. (C) Example of glaciofluvial fan and moraines in the inner fjord. (D) Example of the crag-and-tails and grooves in Cormack Arm.

4.1.3. Proglacial landforms

Two other sets of landforms are identified in the Clyde fjord-cross shelf trough system and characterise the glacial dynamics in front and beyond the receding margin of the ice sheet: iceberg ploughmarks and glaciofluvial fans.

Iceberg ploughmarks - Straight and sinuous V- or U-shaped furrows are observed at varying depths along the fjord-cross-shelf trough system (Figs. 4, 5A and 6A). They are more common on the continental shelf, whereas in the fjord they mostly occur on the sill. They are usually associated with berms or levees on either side and often cross-cut each other. They are 2 m to 10 m-deep, up to 200 m-wide and in some cases can be traced for >5 km. Two predominant orientations can be distinguished for the larger furrows in the outer trough area: 1) near the shelf break, iceberg ploughmarks superimpose the outermost GZW, are observed at depths ranging between 175 and 225 m and have a NNW to SSE orientation; 2) on the stoss side of the second GZW, ploughmarks are observed at depths between 150 and 200 m and have a nearly orthogonal (SW-NE) along-trough orientation (Fig. 4). Some large zones of chaotic scouring patterns are also identified in the outer trough, regardless of shallower surrounding seafloor area (Fig. 4). They are between 1 to 5 km-wide and present both depressions and mound-like morphologies with irregular furrows. The depressions are generally between 2 to 5 m-deep, while the mounds are <2 m-high. The SE flank of the trough is also densely incised by randomly oriented semi-circular pockmarks (Fig. 2A). They are generally <5 m-deep and rarely exceed 100 m-wide.

Due to their straight and sinuous character, V- and U-shaped cross-profiles and chaotic patterns, these furrows are interpreted as ploughmarks – also termed iceberg scours – from iceberg keels associated with calving outlet glaciers during deglaciation (King, 1976; Vorren et al., 1989; Jakobsson et al., 2011; Dowdeswell et al., 2014; Lewis et al., 2016; Brouard and Lajeunesse, 2019a, 2019b). The SSE oriented ploughmarks suggest influence of the Baffin Island Current (BIC), which delivered large icebergs from northern Baffin Bay in the early phases of deglaciation (Andrews et al., 1998; Jennings et al., 2011), whereas the NE orientated iceberg ploughmarks is probably related to ice

427 calving from the Clyde Ice Stream (CIS) margin. The larger chaotic zones possibly
428 correspond to large iceberg (>5 km^2) grounding areas and may have been produced by
429 the ploughing of the seafloor by the keel of larger ice masses that were stuck for long
430 periods of time. Tides and meltwater currents may have caused these iceberg shifts,
431 creating the chaotic pattern. To our knowledge, such features have rarely been identified
432 on continental margins and the genesis presented here remains speculative. The semi-
433 circular pockmarks are interpreted as pits formed by the short-term grounding of icebergs
434 that were semi-buoyant or that turned over, as described by Woodworth-Lynas et al.
435 (1991).

436 *Glaciofluvial fans* - Several smooth and gently sloping fan-shaped morphologies
437 are observed on the flanks of the fjord-cross-shelf trough system, at the mouth of tributary
438 valleys (Fig. 5B, 6B-C). They are generally 1 to 5 km-long and observed at depths
439 between 200 m and 400 m. On their upper reaches, they are dissected by series of parallel
440 15 m-deep channels. On their lower reaches, they are superimposed by transverse 5 m-
441 high and 200 m to 1 km-wide curvilinear ridges.

442 These fan-shaped landforms are interpreted as glaciofluvial fans formed by
443 sediment delivery by glacial meltwaters from adjacent alpine valleys (Powell, 1990;
444 Normandeau et al., 2019). Similar landforms were previously identified from several
445 glaciated locations (Powell, 1990; Lønne, 1995; Dowdeswell and Vásquez, 2013;
446 Normandeau et al., 2019; Brouard and Lajeunesse, 2019a, 2019b). Parallel channels are
447 more common on glacially-fed fans suggesting higher turbidity currents activity used for
448 delivering sediments downslope (Dowdeswell and Vásquez, 2013; Batchelor et al., 2018;
449 Normandeau et al., 2019). Transverse curvilinear ridges observed on foreset beds are
450 crescent-shaped landforms formed by turbidity currents (Normandeau et al., 2019).

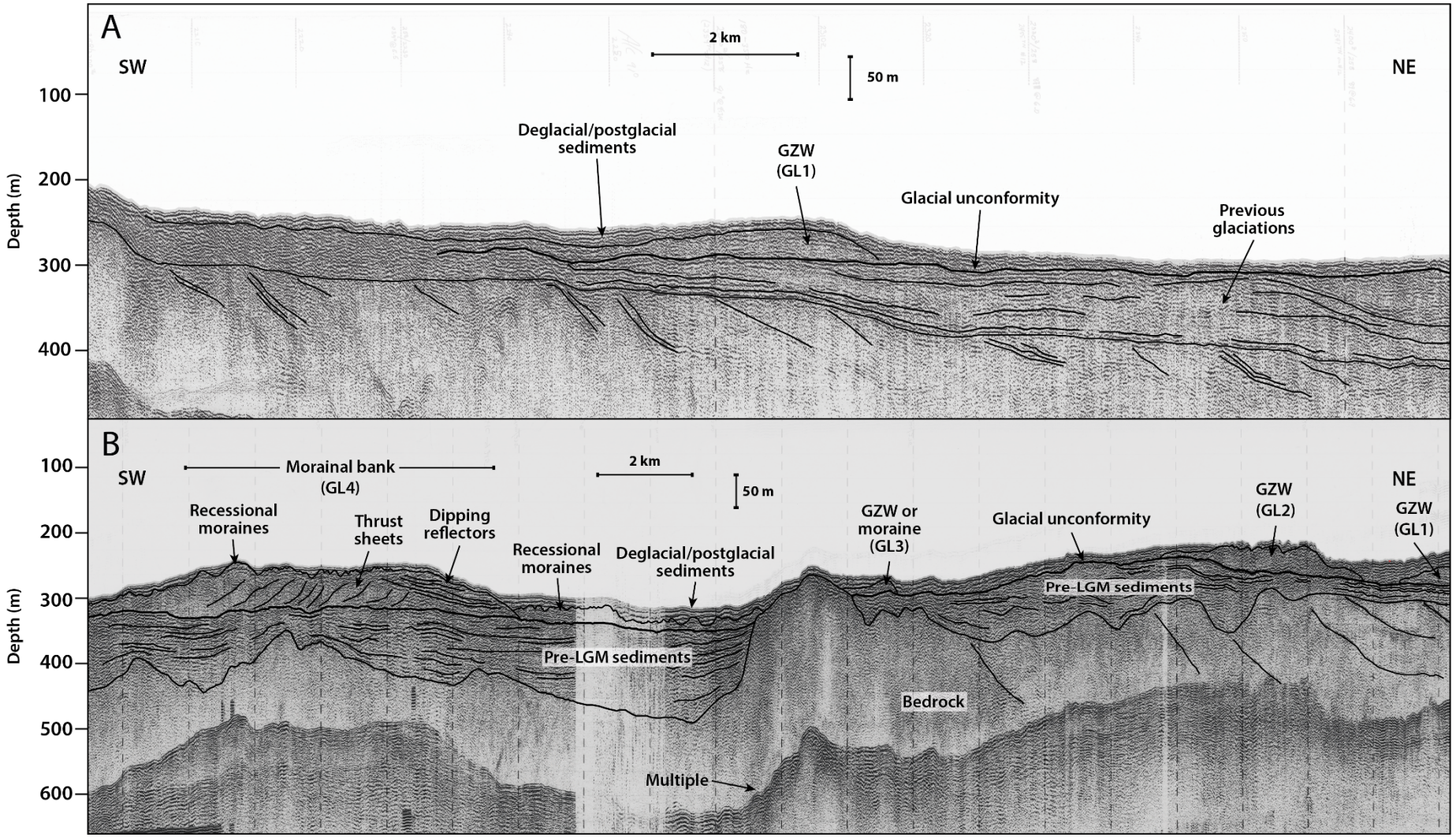

Figure 7 (A) Airgun profile 78029_AG_275_0130 in the outer Clyde Trough showing GL1 and deeply buried GDFs. (B) Airgun profile 80028_AG_RAYT_257_0200 along Clyde Trough showing the sedimentary assemblages. The depth is based on two-way travel time (TWTT) of 1500 m s-1.

4.2. Acoustic stratigraphy

Six acoustic facies (AF) were distinguished from >2,500 km of Parasound profiles in the Clyde fjord-cross-shelf trough system. They were differentiated on the basis of their acoustic signatures, bounding reflectors and internal geometries. Additionally, airgun profiles allow identifying the general stratigraphy in the middle to outer trough and in places the limit between the seaward-dipping strata of the bedrock and Quaternary sediments (Fig. 7). They also allow delineating an erosional surface, which represent an unconformity in the sedimentation sequence. This surface is overlain by an acoustically chaotic to semi-transparent unit, which is in turn overlain by a thin unit (<10 m) of high amplitude parallel reflectors. The erosional surface and overlying sediments identified on airgun data likely represent the complete glaciation/deglaciation cycle, with an ice sheet advance across the continental shelf during the LGM followed by deglacial to postglacial sedimentation. The Parasound profiles however allow for a more in-depth analysis of the different facies represented along the system during deglaciation.

4.2.1. AF0: Acoustically impenetrable to homogenous facies

AF0 is an impenetrable and homogenous acoustic facies and forms the acoustic basement in most profiles (Figs. 8A-D). This facies is not visible in some basins where the attenuation of the acoustic signal in thick sediment prevents penetration. It is internally structureless and is characterised by a weak, high-amplitude rugged upper reflector; in most cases it shows an irregular to hyperbolic geometry.

4.2.2. AF1: Acoustically homogenous, non-conformable facies

AF1 rarely exceeds 5 m thickness and is restricted to the outer trough (Fig. 8A). It is characterised by chaotic and discontinuous acoustic reflectors with occassional hyperbolae near the surface. This facies is acoustically homogenous and exhibits weak lower reflectors. It shows in-filled small-scale (~5 m-deep, ~100 m-wide) V-shaped depressions and a non-conformable configuration.

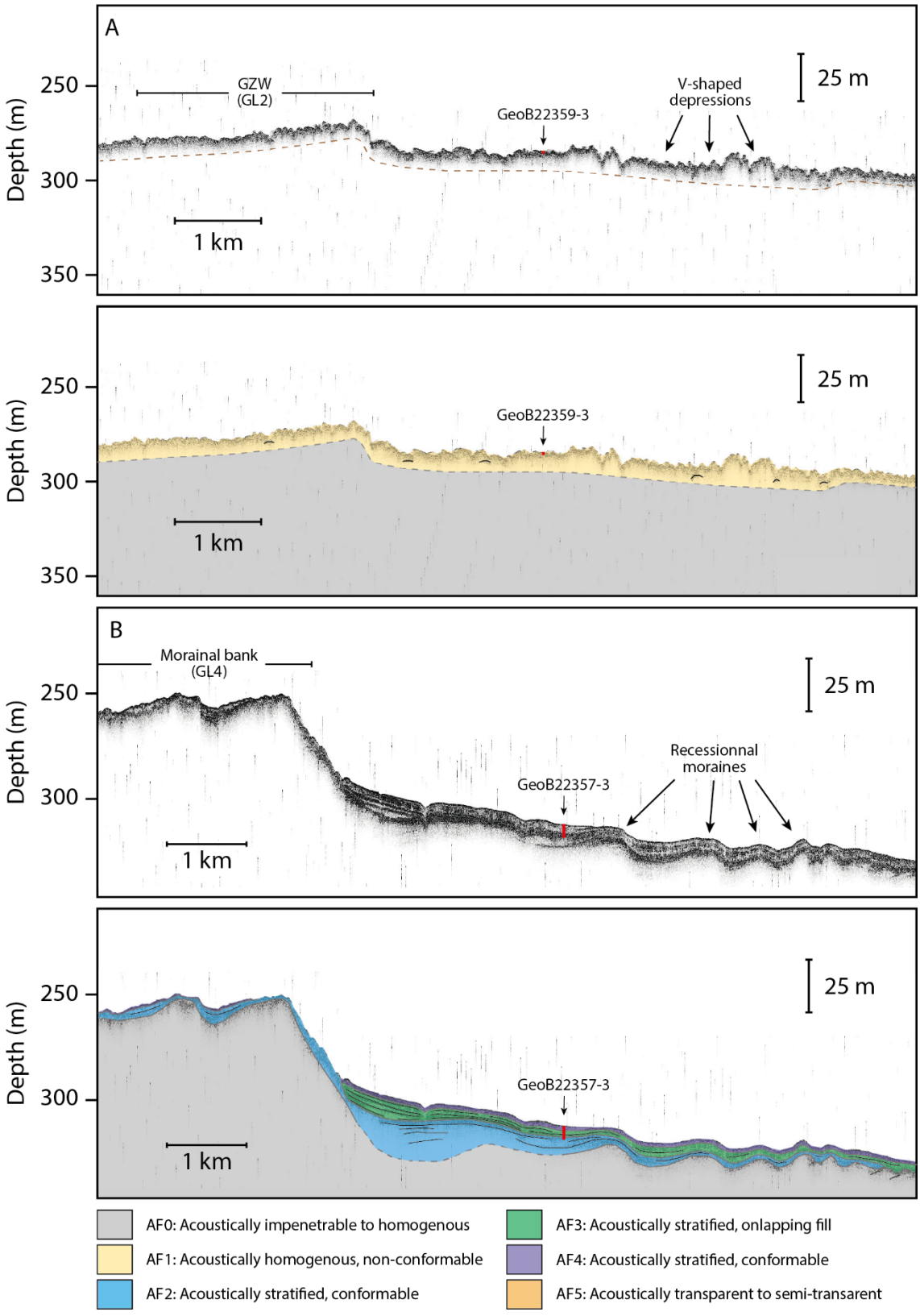

Figure 8 Parasound profiles along the Clyde Inlet fjord-cross-shelf trough system showing the different acoustic facies (Table 1). See Figs. 2 and 3 for location of the profiles. Color coding for the different acoustic facies is the same as the one used for the lithological facies in Fig. 9.

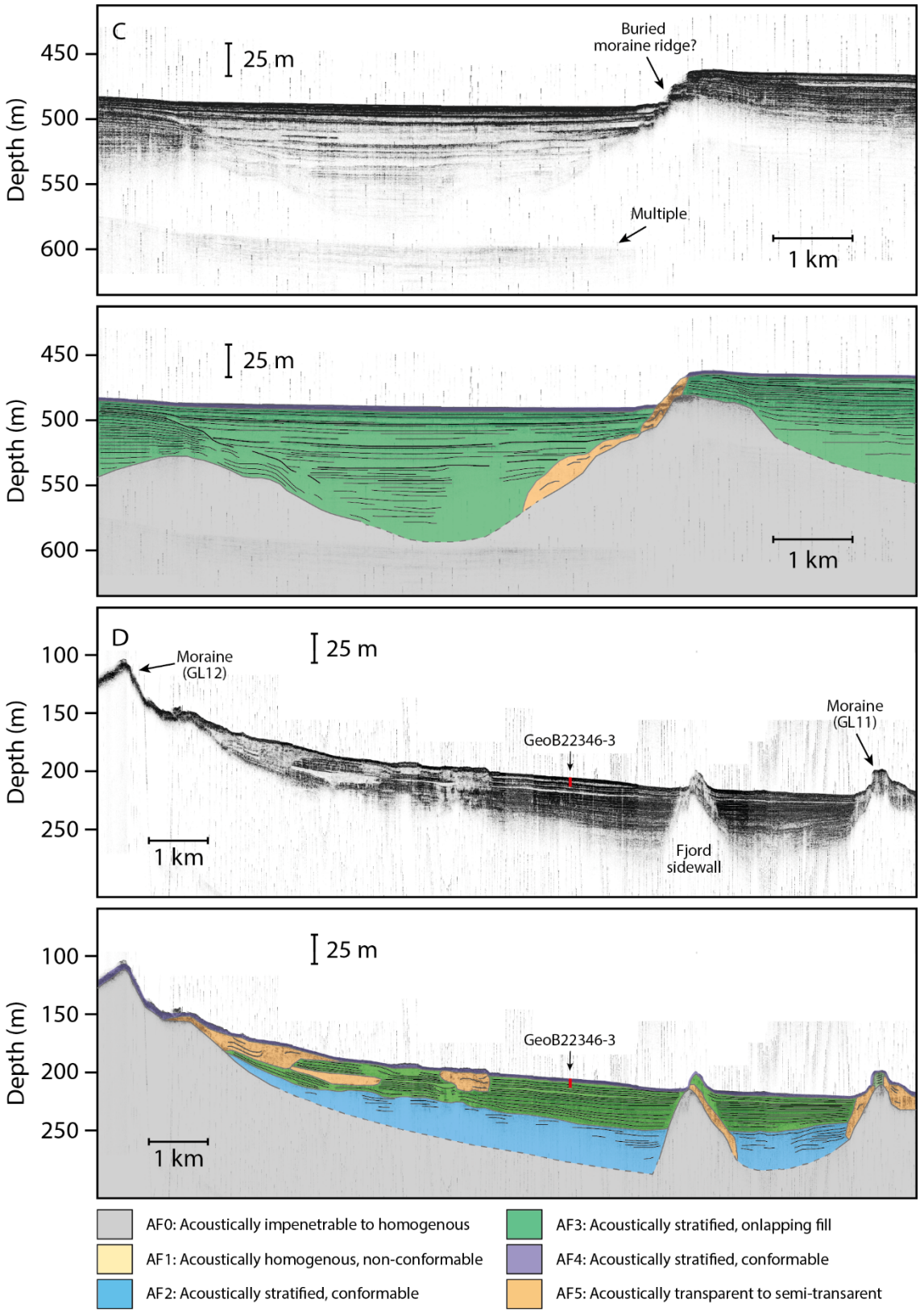

Figure 8 Continued.

4.2.3. AF2: Acoustically stratified, conformable facies

AF2 is an acoustically stratified and conformable facies with a sharp upper reflector and low to medium amplitude parallel to sub-parallel irregularly-spaced internal reflectors (Figs. 8B-D). AF2 drapes the underlying unit and in sometimes exhibits discrete wedge-shape geometries at its lateral boundaries. It is observed over distances of several kilometers in the deeper parts of basins located within the fjord, but is also present at some locations on the inner trough and possibly on the upper slope of the shelf edge (Fig. 7B). AF2 is generally between 5 and 20 m-thick, but reaches >30 m in the inner fjord. This facies is usually observed immediately seaward from grounding line landforms (i.e., GZWs, morainal bank and moraines), although their connection remains elusive.

4.2.4. AF3: Acoustically stratified, onlapping fill facies

AF3 is an acoustically stratified facies with parallel medium to high amplitude reflectors (Figs. 8B-D). It has an onlapping or ponded basin-fill configuration and is interbedded with occasionnal thicker transparent units. This facies is usually between 10 and 40 m-thick, but can reach >75 m in the fjord. Acousticaly chaotic and transparent lenticular sediment bodies are in many cases observed within AF3.

4.2.5. AF4: Acoustically stratified, conformable facies

AF4 is an acoustically stratified facies with parallel, closely spaced high amplitude and opaque reflectors (Figs. 8B-D). It forms a conformable drape of <5 m on the underlying AF3. It characterizes the uppermost sediment bodies deposited in the Clyde fjord-cross-shelf trough system.

4.2.6. AF5: Acoustically transparent to semi-transarent facies

AF5 is an acoustically transparent to semi-transparent chaotic facies with rare or poorly defined internal reflectors (Figs. 8C-D). Sediment bodies showing AF5 usually have an erosive base, an hummocky surface and are either lenticular or taper on slopes.

511 It is often observed interfingered within the stratified AF2 or AF3. It is generally a few
512 meters-thick, but can exceed 10 m-thick locally. AF5 is mostly observed inside the fjord,
513 near slopes and tributary valleys.

514 **4.3. Lithological facies**

515 Glacial lithological facies (LF) were identified from the gravity cores collected in
516 the Clyde Inlet fjord-cross-shelf trough system by combining visual core descriptions,
517 photographs of split cores and XRF data. Five facies and three subfacies were determined
518 based on colour, texture, sedimentary structures (e.g., lamination, bioturbation) and Ca/Ti
519 ratio changes (Fig. 9). Ratios of calcium (Ca) to titanium (Ti) were used for correlation
520 between the cores along the Clyde Inlet transect.

521 *4.3.1. LF1: Unstratified sandy mud with dropstones*

522 LF1 consists of unstratified olive dark gray sandy mud with dropstones and
523 dispersed pebble-sized clasts. This lithofacies shows no or few traces of bioturbation and
524 occurs in the cores of the outer trough. LF1a consists of a gray coarse sandy mud, IRD-
525 rich facies with occasional sand lenses. LF1b has a more reddish brown color with a finer
526 sandy mud matrix and fewer apparent clast. LF1b is only found in core GeoB22359-3 and
527 is characterized by a high peak in Ca/Ti ratio.

528 *4.3.2. LF2: Poorly sorted diamicton*

529 LF2 only occurs at the base of core GeoB22357-3 and consists of dark gray
530 weakly stratified, poorly sorted muddy-sand matrix diamicton. It is characterized by thick
531 horizons (50-75 cm) of abundant sub-angular to sub-rounded clasts ranging from granules
532 to pebbles, resulting in relatively higher and more chaotic peaks of Ca/Ti ratio. Diamicton
533 beds of LF2 have conformable bedding contact and are interbedded with massive to
534 laminated and faulted silty mud beds of LF3.

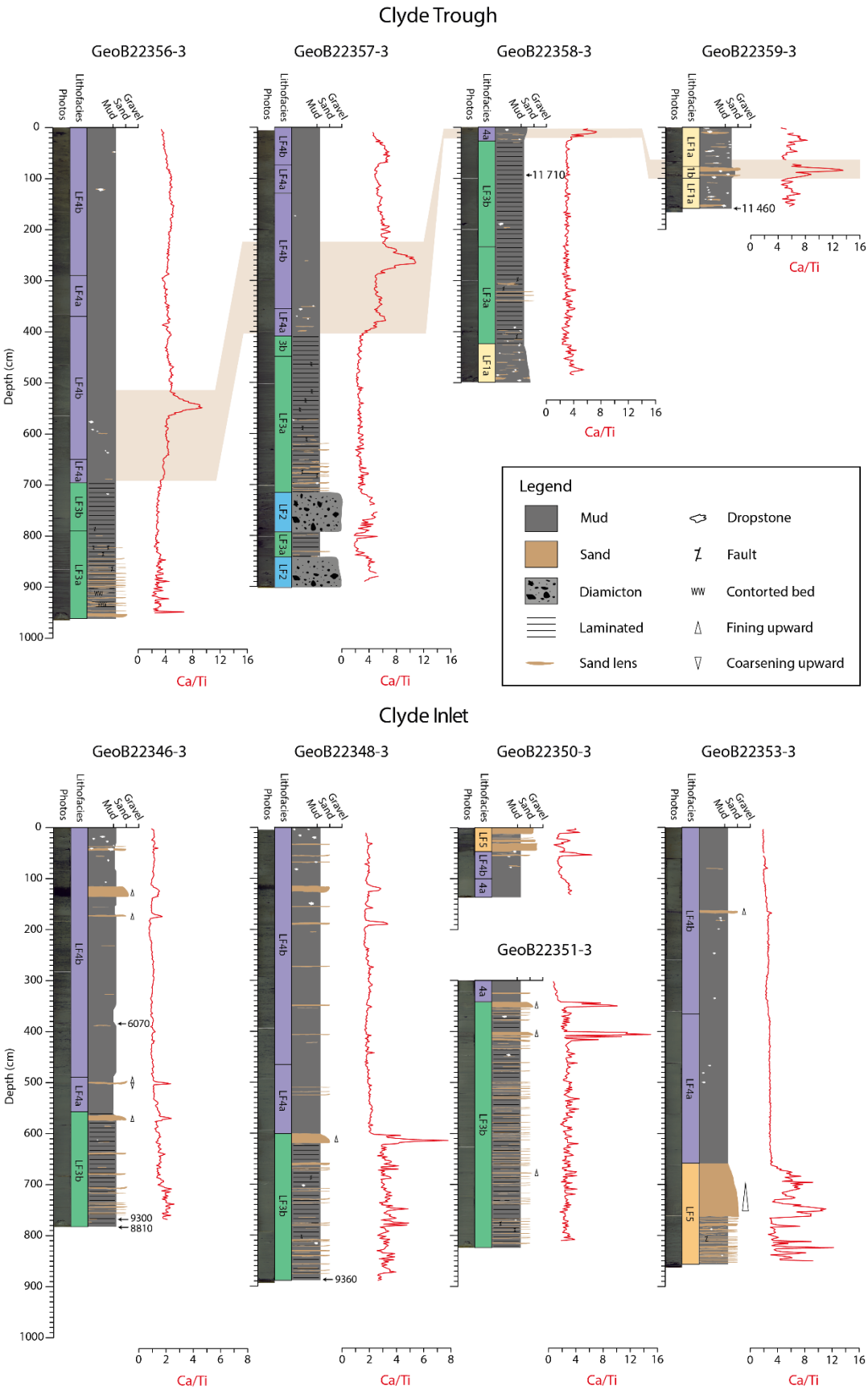

Figure 9 Simplified lithological logs, Ca/Ti ratios and calibrated radiocarbon ages of sediment cores collected along the Clyde Inlet fjord-cross-shelf trough system. Note that Ca/Ti ratios have a different scale for GeoB22344-3, GeoB22346-3 and GeoB22348-3. Color coding for the different lithological facies is the same as the one used for the acoustic facies in Fig. 8.

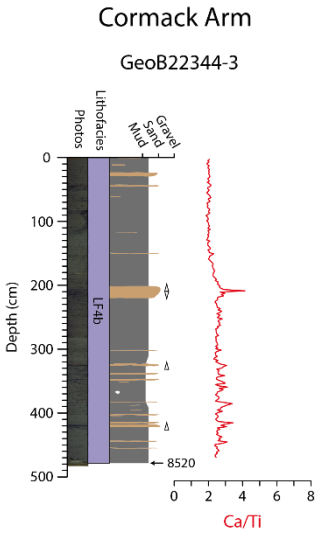

Figure 9 Continued.

4.3.3. LF3: Laminated mud with sandy layers

LF3 is a laminated gray to dark gray silty mud characterised by a lack of bioturbation and the presence of scattered angular to sub-angular clasts. It also contains individual thin sand laminae that has sharp basal contacts. The sand layers are coarser and thicker at the base of the unit, defining an overall fining upward trend. LF3a is defined by the presence of faulting, as well as more irregular and prominent laminae. LF3b shows no faulting but contains faint thinner beds of coarser sediments. Curves of Ca/Ti ratios from LF3b are chaotic with numerous peaks generally corresponding to coarser laminae. The laminae become less prominent and more spaced upward at the transition from LF3a to LF3b.

4.3.4. LF4: Massive bioturbated silty mud

LF4 consists of massive olive gray, bioturbated silty mud and occur at the top of most cores, except GeoB22350-3 and GeoB22359-3. This lithofacies generally contains black mottles and few clasts. The transition with the underlying unit is gradational; LF4a is weakly bioturbated, while LF4b contains high concentrations of bioturbation and black mottles. Ca/Ti ratios in the fjords are relatively low with distinct peaks representing sandy

559 layers. In the trough, these ratios are higher and more irregular with peaks representing
560 longer events or of bigger magnitude.

561 *4.3.5. LF5: Unstratified sand*

562 LF5 is characterized by unstratified gray coarse sand with lenses of olive gray
563 silty mud and occur only at the top of core GeoB22350-3 and at the base of core
564 GeoB22353-3. This unit rest on LF4 and shows traces of bioturbation in the silty mud
565 lenses. Ratios of Ca/Ti in LF5 are characterized by chaotic and irregular peaks.

566 **4.4. Correlation of acoustic stratigraphy and lithological facies**

567 Combining the acoustic stratigraphy and lithological facies allows drawing the
568 sedimentary architecture of the Clyde fjord-cross-shelf trough system. Table 2 presents a
569 summary of the acoustic stratigraphy and lithofacies descriptions in their context of unit
570 correlations.

571 *4.4.1. Unit 0: Bedrock or ice-contact sediments*

572 Based on its stratigraphic position, acoustic appearance and rugged upper
573 reflector, Unit 0 represents bedrock and/or ice-contact sediments (Syvitski and Shaw,
574 1995; Streuff et al., 2018). Due to the absence of penetration in coarse sediments, it is
575 usually difficult to differentiate between the two types on acoustic profiles (Streuff et al.,
576 2018; Hogan et al., 2020). Nevertheless, Mesozoic to Tertiary sedimentary bedrock is
577 recognizable on airgun profiles by seaward-dipping strata, whereas ice-contact deposits
578 have a chaotic internal signature (Fig. 7). These profiles also reveal an unconformity that
579 lies above >50 m of undifferentiated Quaternary sediments.

580 *4.4.2. Unit 1: Iceberg-influenced sedimentation*

581 Unit 1, comprising AF1 and LF1, is interpreted as iceberg-influenced
582 sedimentation, with ploughing and subsequent infilling by ice rafted sediments
583 (Woodworth-Lynas et al., 1991; Arosio et al., 2018; Callard et al., 2018; Streuff et al.,

584 2018; Olsen et al., 2022). Hyperbolic signals present in this facies are characteristic of
585 point-source diffractions from dispersed cobbles and boulders (Arosio et al., 2018;
586 Callard et al., 2018). The unstratified structure and high pebble-sized clasts content
587 suggest that iceberg calving was an important sediment source (Dowdeswell et al., 1994,
588 2000; Ó Cofaigh and Dowdeswell, 2001; Ó Cofaigh et al., 2013a; Hogan et al., 2016;
589 Sheldon et al., 2016). Its occurrence in heavily iceberg-disturbed area, as shown by
590 multibeam bathymetry (Fig. 4), is consistent with this interpretation. The reddish brown
591 color and the high Ca/Ti ratio of LF1b might correspond to a predominantly detrital
592 carbonate input from northern Baffin Bay – possibly BBDC-0 (Simon et al., 2014;
593 Jackson et al., 2017; Jenner et al., 2018; Lévesque et al., 2020).

594 *4.4.3. Unit 2: Glacigenic debris-flows*

595 Based on its conformable geometry, stratified acoustic signature and sandy
596 matrix-supported diamicton facies, AF2 and LF2 are interpreted as glacigenic debris-
597 flows likely sourced during stillstands of the ice margin (Powell, 1990; Powell and Alley,
598 1997; King et al., 1998; Ó Cofaigh and Dowdeswell, 2001; Flink and Noormets, 2018).
599 The alternating nature of LF2 with the laminated/faulted mud of LF3 is consistent with
600 an origin of distinct pulses of glacigenic debris-flows interbedded with meltwater plumes
601 (Ó Cofaigh et al., 2013a; Callard et al., 2018; Jenner et al., 2018; Prothro et al., 2018).
602 High sand and gravel content often indicate an ice-proximal sedimentation located within
603 a few kilometers of the grounding line, which requires a stable ice margin over a period
604 of years to decades in case of a thick accumulation (Ó Cofaigh et al., 2008; Dowdeswell
605 et al., 2015; Callard et al., 2018; Prothro et al., 2018). Comparable facies have commonly
606 been identified near glacier-influenced submarine fans and are inferred to be related to
607 the remoblization of glacigenic debris at the grounding line by abundant subglacial
608 meltwater discharge (Syvitski, 1991; King et al., 1998; Ó Cofaigh et al., 2013b;

609 Dowdeswell et al., 2015). The occurrence of such facies at a relatively short distance (<2
610 km) from former major grounding line positions in the Clyde fjord-cross-shelf trough
611 system therefore support this interpretation.

612 *4.4.4. Unit 3: Ice-proximal glaciomarine sedimentation*

613 Unit 3, comprising AF3 and LF3, is interpreted as stratified ice-proximal
614 glaciomarine sedimentation (Ó Cofaigh and Dowdeswell, 2001; Hodgson et al., 2014;
615 Normandeau et al., 2017; Brouard and Lajeunesse, 2019a; Trottier et al., 2020; Olsen et
616 al., 2022). The well-preserved laminations suggest fallout sediment deposition from
617 meltwater plumes (Syvitski, 1991; Ó Cofaigh and Dowdeswell, 2001; Sheldon et al.,
618 2016; Jenner et al., 2018; Callard et al. 2020; Olsen et al., 2022). Laminae probably
619 correspond to seasonal changes in sedimentation, where finer layers result from reduced
620 subglacial meltwater input during winter (Flink and Noormets, 2018; Prothro et al., 2018).
621 The sand layers with sharp basal contacts correspond to deposition by turbidity currents
622 or turbid meltwaters sourced from the ice margin (Sheldon et al., 2016; Olsen et al., 2020).
623 Dispersed clasts, indifferentially found in fine- or coarse laminae are interpreted as ice-
624 rafted debris (IRD). The occurrence of randomly dispersed IRDs indicates that rain-out
625 from icebergs was a minor sedimentation process contributing to LF3 (Syvitski, 1991;
626 Sheldon et al., 2016) and/or accumulation rates were high, with dilution of the IRD signal
627 (Syvitski and Shaw, 1995; Dowdeswell et al., 2000; Olsen et al., 2022). The latter
628 interpretation is in agreement with the lack of bioturbation (Ó Cofaigh and Dowdeswell,
629 2001; Sheldon et al., 2016; Callard et al. 2020). Rapid sediment loading causing minor
630 submarine slope failures may explain the abundant occurrence of faults in LF3a (Callard
631 et al., 2018; Allaart et al., 2020). The decrease of the thickness and grain size of the
632 laminae and the disappearence of faulting in LF3b together reflect a progressively distant
633 marine terminating ice margin, representing ice-proximal to distal glaciomarine

sedimentation (Ó Cofaigh and Dowdeswell, 2001; Dowdeswell et al., 2015; Streuff et al., 2017; Callard et al., 2018, 2020; Jenner et al., 2018; Allaart et al., 2020).

4.4.5. Unit 4: Ice-distal hemipelagic sedimentation

The acoustic appearance of AF4 and LF4 corresponds to typical ice-distal hemipelagic sedimentary systems. Comparable acoustic facies have been identified in polar regions and are usually deposited by meltwater run off, tidal processes and, in a lesser extent, ice rafting sedimentation (Syvitski, 1991; Syvitski and Shaw, 1995; Hogan et al., 2016, 2020; Normandeau et al., 2017; Callard et al., 2018; Arosio et al., 2018; Streuff et al., 2018). The sediments show little to no ice-rafting debris (IRDs), suggesting a distal or terrestrial ice margins (Syvitski, 1991; Syvitski and Shaw, 1995; Sheldon et al., 2016; Callard et al., 2018; Olsen et al., 2020, 2022; Syvitski et al., 2022). The transition from weakly (LF4a) to intensively (LF4b) bioturbated mud essentially represents decreasing sedimentation rates with landward retreating glacier fronts (Callard et al., 2018; Jenner et al., 2018). The heavy bioturbation indicates hemipelagic sedimentation, similar to that of today.

4.4.6. Unit 5: Turbidites or mass-movement deposits

Based on the transparent acoustic signature of AF5 and the unstratified sandy structure of LF5, unit 5 is interpreted as a coarse-grained unit from various high-energy sources such as turbidites or mass-movement deposits, which is supported by its occurrence at the foot of slopes or in front of glacially-fed tributary valleys (Syvitski and Shaw, 1995; Streuff et al., 2017; Hogan et al., 2020; Olsen et al., 2022). The presence of bioturbated mud lenses in between beds of coarse sand suggest that Unit 5 is not the continuity of Unit 4, but they are rather intermittent. The position of the coring sites in front of major valley deltas may indicate distinct cohesionless mass-movement deposits from remobilized coastal sediments (Gilbert et al., 1990).

659 **Table 2** Description of sedimentary units identified in the sub-bottom profiles data and sediment cores from the Clyde fjord-cross-shelf trough system. Color coding for the
660 different units is the same as the one used for the acoustic facies in Fig. 8 and the lithological facies in Fig. 9.
661

Unit	Acoustic facies	Example	Description	Lithological facies	Example	Description	Interpretation
U0	AF0	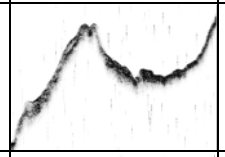	Acoustically impenetrable. Homogenous and structureless. High-amplitude upper reflector. Occasional hyperbolas.				Acoustic basement (bedrock/ice-contact)
U1	AF1	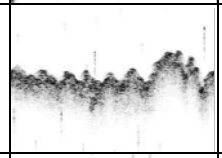	Semi-transparent and chaotic. Discontinuous and homogenous reflectors. Non conformable geometry.	LF1		Unstratified olive dark gray sandy mud. Randomly disseminated pebble-sized clasts. Few traces of bioturbation.	Iceberg-influenced sedimentation
U2	AF2	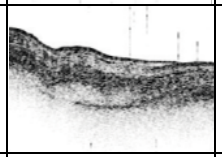	Acoustically stratified. Low to medium amplitude parallel to sub-parallel internal reflectors. Conformable geometry.	LF2		Dark gray muddy-sand matrix diamicton. Weakly stratified and poorly sorted. Dispersed sub-angular to sub-rounded clasts. Interbedded with LF3.	Glacial debris-flows
U3	AF3	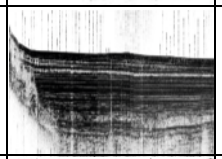	Acoustically stratified. Medium to high amplitude parallel internal reflectors. Basin fill (ponded) or onlapping geometry.	LF3		Laminated gray to dark gray silty mud. Sand laminae with sharp basal contact. Lack of bioturbation. Occasional clasts. Presence of faults at the base.	Ice-proximal glaciomarine sedimentation
U4	AF4	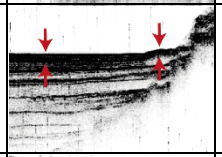	Acoustically stratified. High amplitude parallel and closely-spaced opaque reflectors. Conformable geometry.	LF4		Massive olive gray silty mud. Moderately to heavily bioturbated. Presence of black mottles and rare clasts. Gradational transition from LF3.	Ice-distal hemipelagic sedimentation
U5	AF5	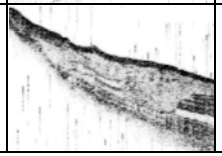	Acoustically transparent to semi-transparent. Chaotic with rare internal reflectors. Hummocky surface and lenticular shaped geometry.	LF5		Unstratified gray coarse sand with bioturbated lenses of olive gray silty mud.	Turbidites and mass-movement deposits

662

4.5. Radiochronology

Seven ages were obtained from radiocarbon dated material collected from the sediments cores (Table 3).

Table 3 Radiocarbon and calibrated radiocarbon ages from material collected in sediment cores.

Core number	Depth in core (cm)	Dated material	Laboratory ID	^{14}C age yr BP	Calibrated age yr BP (2σ)
GeoB22344-3	472-483	Mixed benthic foraminifera	AWI-2620.1.1	8280 ± 90	8520 (8280-8840)
GeoB22346-3	387	Shell fragment	AWI-1726.1.1	5930 ± 50	6070 (5900-6250)
GeoB22346-3	765	Shell fragment	AWI-1727.1.1	8900 ± 190	9300 (8770-9850)
GeoB22346-3	766-783	Mixed benthic foraminifera	AWI-2619.1.1	8510 ± 100	8810 (8500-9120)
GeoB22348-3	888-896	Mixed benthic foraminifera	AWI-2618.1.1	8940 ± 100	9360 (9050-9600)
GeoB22358-3	92	Shell fragment	AWI-1728.1.1	10670 ± 177	11710 (11190-12290)
GeoB22359-3	156-166	Mixed benthic foraminifera	AWI-2617.1.1	10500 ± 100	11460 (11170-11800)

The AMS ^{14}C ages were calibrated within the age-depth modelling process, using the online software Calib 8.2 with the Marine20 radiocarbon age calibration curve (Heaton et al., 2020). A local reservoir correction (ΔR) of 81±18 was used to account for the regional offset of the world ocean ^{14}C age, as determined by Pieńkowski et al. (2022).

In Clyde Trough, at the base of core GeoB22359-3, mixed benthic foraminifera in iceberg-influenced sediments (LF1) provided an age of 11.5 ka cal. BP. A shell fragment from ice-proximal glaciomarine sediments (LF3), at 92 cm from the top of core GeoB22358-3, yielded an age of 11.7 ka cal. BP. These ages in deglacial sediments provide a minimum age for the deglaciation of the outer trough (Fig. 2). However, the age in GeoB22358-3 shows that it is most likely an underestimation of the deglaciation as the sample was collected near the top of the core.

In the inner Clyde Inlet (Fig. 3), three ages were provided from samples collected in ice-proximal glaciomarine sediments (LF3) from the base of two sediment cores. The sample at the base of sediment core GeoB22348-3, taken approximately 25 km from the fjord head, revealed an age of 9.4 ka cal. BP. The base of sediment core GeoB22346-3, taken 10 km from the fjord head, yields an age of 8.8 ka cal. BP. A shell fragment near the base of GeoB22346-3, yielding an age of 9.3 ka cal. ka BP, was rejected because it was inconsistently older than the benthic foraminifera sample taken a few centimeters below. The shell fragments could have been reworked, as the age range is consistent with

686 a reworked shell found in a delta at the fjord head and another one found in a nearby
687 tributary valley (Briner et al., 2007). Therefore, the benthic foraminifera sample is
688 favoured as being the most reliable age available for the base of that core. An age of 6.1
689 ka cal. BP was also obtained from a shell fragment at 387 cm downcore, in ice-distal
690 glciomarine sediments (LF4).

691 Similarly, a foraminifera sample collected in ice-distal glaciomarine sediments
692 (LF4) from the base of sediment core GeoB22344-3 yielded an age of 8.5 ka cal. BP. It
693 thus provides a minimum age for full deglaciation of Cormack Arm.

694 # 5. Discussion

695 ## 5.1. Extent and retreat of the LIS margin

696 The analysis of the multibeam bathymetry, acoustic profiles and lithological
697 facies allowed the identification of landforms and sedimentary assemblages that are
698 typical of high-latitude fjord-cross-shelf trough systems (e.g., Praeg et al., 2007;
699 Winsborrow et al., 2010; Ó Cofaigh et al., 2013b; Sheldon et al., 2016; Slabon et al., 2016;
700 Brouard and Lajeunesse, 2017; Ottesen et al., 2022). They provide valuable information
701 on the maximal extent of the LIS margin and its retreat patterns along the entire Clyde
702 fjord-cross-shelf trough system. However, deglacial ages on the shelf and nearby fjords
703 of Baffin Island are scarce and correlations with other systems is therefore tentative. The
704 radiocarbon dated horizons of the cores are stratigraphically too shallow to construct
705 reliable age extrapolations to the base of the deglacial units. Nevertheless, they represent
706 minimum-limiting ages at the coring sites and thus provide some constraints on ages of
707 the deglaciation patterns we present. The compatibility with land-based studies provides
708 independent corroboration that allow us to draw a more accurate chronology of the
709 deglaciation for the Clyde fjord-cross-shelf trough system (Fig. 10).

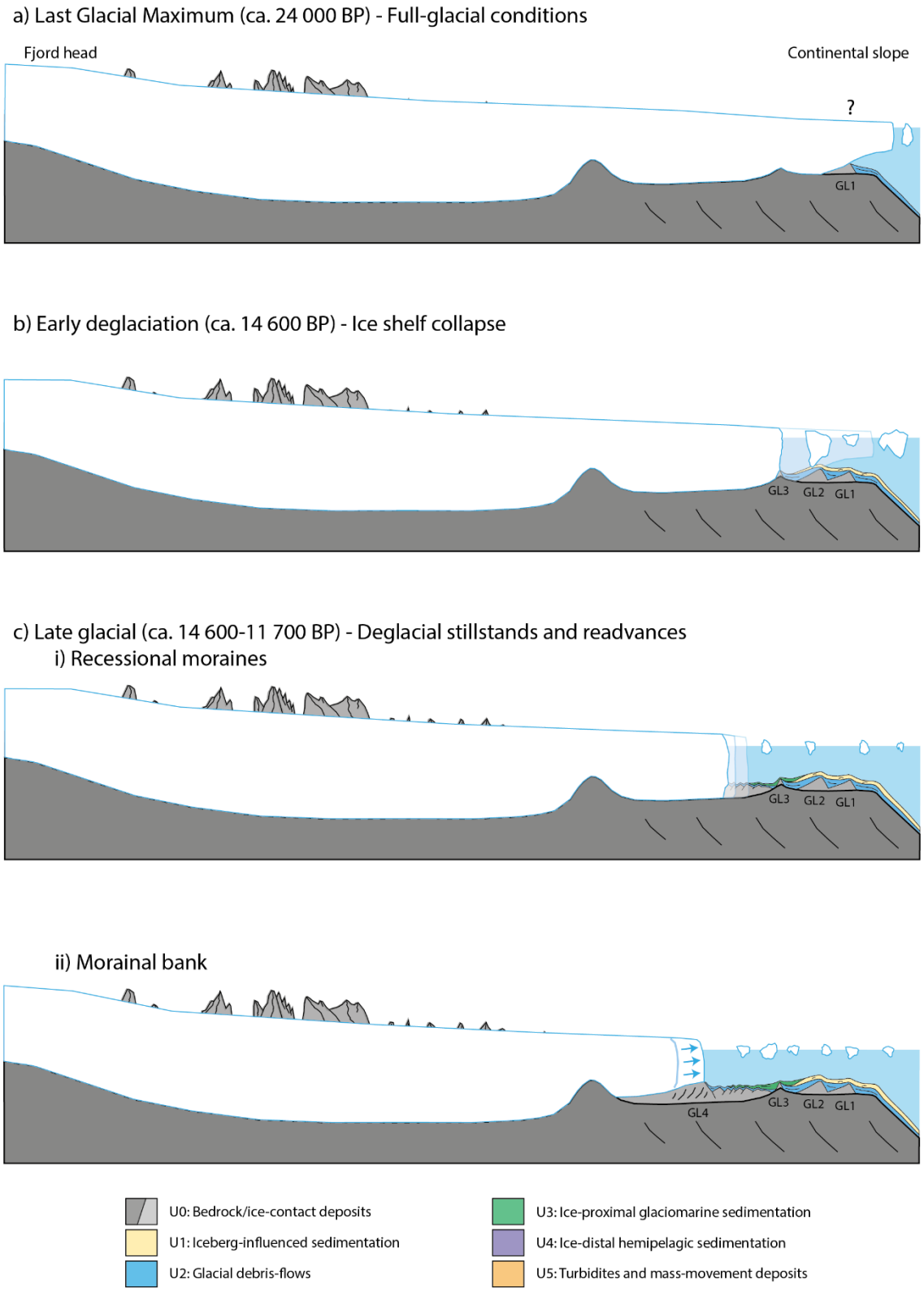

710

711 **Figure 10** Schematic representation of the ice dynamics on the shelf corresponding to the different stages
712 of ice retreat during deglaciation in Clyde fjord-cross-shelf trough system.

d) End of Younger Dryas (11 700 BP) - Fjord mouth sill stillstand

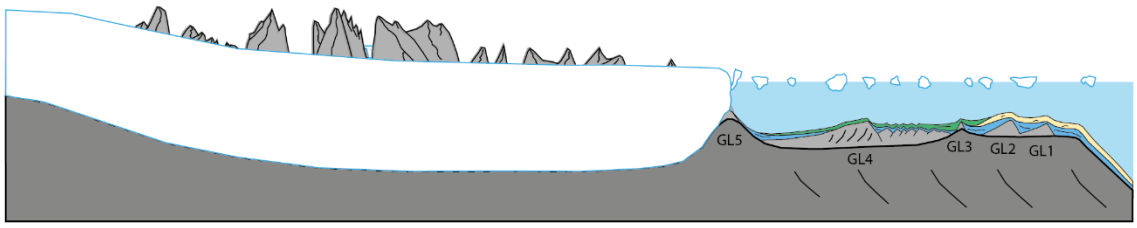

e) Early Holocene (11 700-9500 BP) - Fast retreat into the fjord

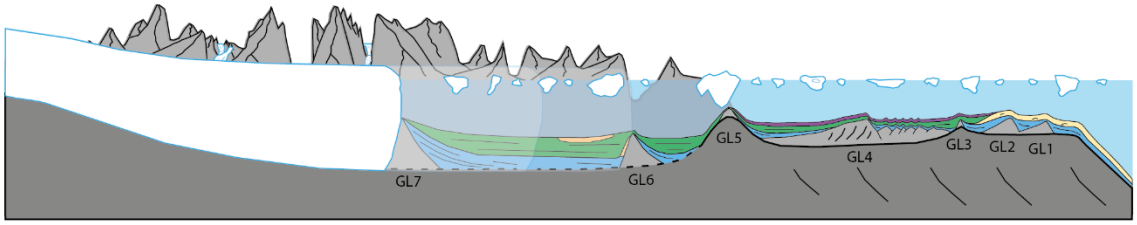

f) Cockburn substage (9500-8000 BP) - Fjord head stillstands or readvances

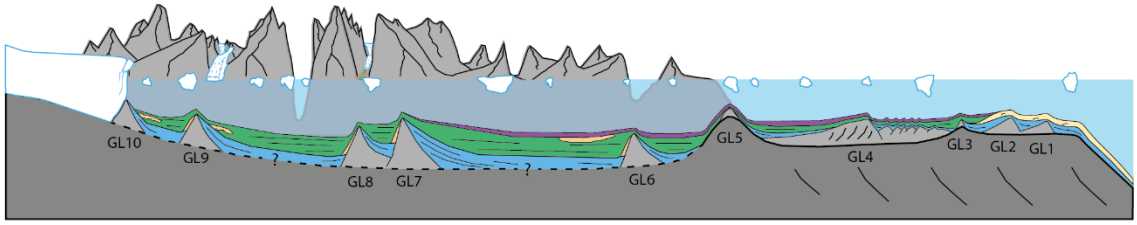

g) Late Holocene (8000 BP - Now) - Paraglacial conditions

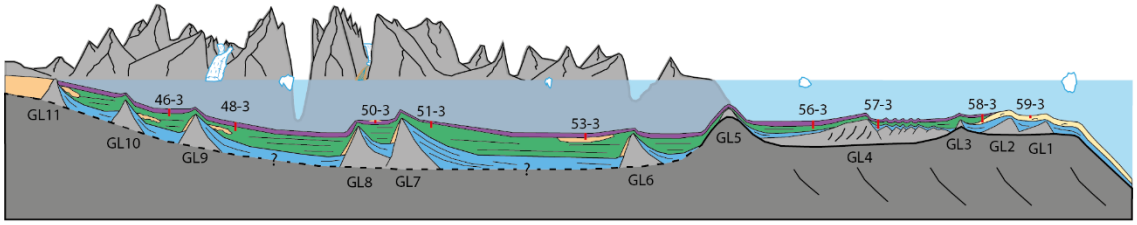

713

714 **Figure 10** Continued.

715

5.1.1. LGM extent and collapse of the Clyde ice shelf

Couette et al. (2022) asserted that the LIS did not reach the shelf break in Clyde Trough on the basis of geomorphological, sedimentological and glaciological evidence. They argued that the absence of gullies on the trough mouth fan and glacial lineations in the outer trough – which are both diagnostic of a grounded ice margin extending at the shelf break – suggest that the LIS had a receded position in Clyde Trough. It is also possible that the extensive iceberg ploughmarks observed in the outer trough have obscured any landforms that provide evidence for the LIS margin reaching shelf break during the LGM. In the absence of such evidence, the GZWs observed near the shelf edge are therefore identified as the most probable maximal position of the LIS in Clyde Trough during the LGM (Fig. 10a). The onset of deglaciation around Baffin Bay appears to have occurred between 16 and 14.6 ka cal. BP on eastern Baffin Island (Jennings, 1993; Briner et al., 2007; Margreth et al., 2017) and western Greenland (Sheldon et al., 2016; Jennings et al., 2017). This timing for the deglaciation of the shelves is in agreement with cosmogenic exposure dating from the Clyde Foreland, where deglaciation is interpreted to have started at ~15 ka BP (Briner et al., 2005). As no direct dating has yet yielded absolute ages on these landforms, it can not be asserted with certitude which of the two GZWs, if any, represent the LGM maximal extent. The change in orientation and density of iceberg ploughmarks suggest that the CIS margin was possibly grounded at GL2 during the early phases of deglaciation, when numerous icebergs were released into Baffin Bay and transported via the Baffin Island Current (Andrews et al., 1998). The large iceberg ploughmarks parallel to the trough on the stoss side of GL2 and the IRD-rich facies in the outer trough are, in turn, evidence of a period of extensive iceberg release provoked by the collapse of the Clyde ice shelf and rapid retreat of the CIS (Fig. 10b). Therefore, this period of rapid ice decay might correspond to Meltwater Pulse 1a (MWP-1a – 14.6-14.0 ka cal. BP; Carlson, 2009; Harrison et al., 2018; Lin et al., 2021), which coincides with

742 the release of icebergs and detrital carbonate-rich sediments into Baffin Bay (BBDC layer
743 1 – ~14.2-13.7 ka cal. BP) from northwestern Greenland and the eastern CAA (Andrews
744 et al., 1998; Simon et al., 2012, 2014; Jackson et al., 2017).

745 It is unclear why the LIS margin did not reach the shelf break in Clyde Trough, as
746 ice extended across the continental shelf in Lancaster Sound as well as in the Buchan and
747 Scott trough systems of northeastern Baffin Island (Li et al., 2011; Brouard and
748 Lajeunesse, 2017). Recent studies (i.e., Miller et al., 2002; Margreth et al., 2017) also
749 suggest that the ice margin did not reach the shelf break on Cumberland Peninsula
750 (eastern Baffin Island). The position of the ice margin at the LGM along the coast of
751 eastern Baffin Island was most probably variable. Clyde Trough might represent a zone
752 of transition between the "Big ice" model of northeastern Baffin Island and the "Just-
753 Right ice'' model observed on Cumberland Peninsula (see Miller et al., 2002). This
754 intermediate position was also reported in Sam Ford Trough – just north of Clyde Trough
755 –, although this system is considered to have been occupied by slow flowing ice during
756 the LGM (Brouard and Lajeunesse, 2017). Slower flowing ice could also explain the
757 receded position of the ice margin in Clyde Trough, as sparse and undefined glacial
758 lineations in the outer trough suggests limited ice streaming activity at the LGM.
759 However, the lack of glacial lineations on the outer trough possibly reflects the significant
760 disturbance of the seafloor by iceberg ploughmarks. Nonetheless, it is worth noting that
761 a slow ice flow regime was observed for the adjacent Clyde Lowlands, where ice flowing
762 through Ayr Lake was non-erosive and slow flowing in its outermost part (Briner et al.,
763 2005). The opening/diffluent configuration of the outer trough could have favored
764 reduced ice velocity, thus limiting the formation of glacial lineations at the base of the ice
765 stream. A reduced ice velocity could result from a limited catchment size due to the
766 presence of more competent ice stream system on either side of the Clyde fjord-cross-

767 shelf trough system. Similar observations have been made on the shelf of northeastern
768 Baffin Island, where piracy of ice drainage basins controlled the volume of ice flow into
769 Sam Ford Trough system (Brouard and Lajeunesse, 2019c). Additionally, the CIS was
770 sustained by cold-based ice on the banks in front of the Clyde and Aston lowlands (Briner
771 et al., 2005). GZWs geometry indicates that cold-based ice also had a receded position on
772 the inter-trough on both sides of Clyde Trough. Sediment assemblages on the Baffin slope
773 further support that position, at least for the later part of the LGM (Jenner et al., 2018).
774 Stacked tills underneath GL1 indicate that some earlier glaciations were, however, more
775 extensive, as previously proposed by various authors for Arctic Canada (i.e., Miller et al.,
776 1977; England et al., 2009).

777 *5.1.2. Slow late glacial retreat on the shelf*

778 The absence of large GZWs in the middle and inner trough suggests that the ice-
779 retreat following the initial breakup of the CIS occurred in a steady fashion as shown by
780 sets of recessional moraines (Fig. 10c i). This slow retreat pattern differs from
781 observations from other trough systems of northeastern Baffin Island, where deglaciation
782 occurred in a more stepwise pattern with prolonged stillstands indicated by GZWs
783 (Brouard and Lajeunesse, 2017). This deglaciation pattern, situated on the retrograde
784 sloping part of the trough, is uncommon compared to other global occurrences which
785 generally present few stillstand indicators and are usually attributed to a rapid ice margin
786 retreat (Weertman, 1974; Favier et al., 2014; Wise et al., 2017). Similar variations in style
787 and rate of ice retreat along a continental shelf has also been observed on the Antarctic
788 Peninsula (Dowdeswell et al., 2008; Ó Cofaigh et al., 2014 and references therein) and
789 may thus reflect the influence of local controls (i.e., bathymetry and topography) on ice
790 dynamics of northeastern Baffin Island (see section 5.2).

The morainal bank (GL4) in the middle trough indicates a stage of ice margin readvance and short-term stabilization during the generally slow deglaciation of the trough (Fig. 10c ii). It aligns roughly with lateral moraines dated by Briner et al. (2005) near Patricia Bay, indicating that this event occurred at ~12.5 ± 0.7 ka. It is therefore probable that an ice margin readvance during the colder Younger Dryas (~12.9 – 11.7 ka BP) favoured the formation of the morainal bank. Regardless of their genesis as glaciotectonic push-and-thrust or crevasse-squeezed ridges, the transverse and zigzag-shaped ridges on the morainal bank suggest readvance of the LIS margin. These landforms may reflect warm-based fast flow conditions changing to cold-based freeze-on conditions near the ice margin (Christofferson and Tulaczyk, 2003; Laberg et al., 2009). Cold-based conditions at the ice-margin can be caused by ice thinning, fast downward advection of cold surface ice or basal freezing of the ice stream termination (Christofferson and Tulaczyk, 2003). Zigzag-shaped ridges have also been associated to ice readvances on the Værøy and Røst morainal banks, in northern Norway (Laberg et al., 2009). The Røst morainal bank is also seismically similar to the middle trough morainal bank with its folded reflectors at the front and the irregular thrusted sheets in its core (Laberg et al., 2009). Folding and thrusting of sediment sheets by glaciotectonism (Fig. 7B), which is caused by movements at the front of the glacier (i.e., a readvance of the LIS margin), have been speculated to increase the height of ice-contact deposits (Powell, 1990; Lønne, 1995; Lyså and Vorren, 1997).

The moraine system on top of a bedrock sill at the fjord mouth (GL5) indicates that the ice margin stabilized here for a short period (Fig. 10d). In the cores collected along Clyde Trough, ages of 11.7 and 11.5 ka cal. BP below the transition from ice-proximal glaciomarine sediments to ice-distal hemipelagic sediments provide a minimal age for the ice margin retreat into the fjord. This transition is also marked by a peak in

816 Ca/Ti in the shelf cores, corresponding to an increase in detrital carbonate-rich sediments
817 (BBDC layers) from northern Baffin Bay. This increase was also recorded along West
818 Greenland and the onset of this event was dated at ~11.6 ka cal. BP (Jennings et al., 2014,
819 2017). This timing for ice retreat from the fjord-mouth at the onset of the Holocene is
820 further supported by data from Scott Trough suggesting ice-distal sedimentation from ~12
821 ka cal. BP (Osterman and Nelson, 1989). Cosmogenic exposure dating from the
822 continental domain indicates that the LIS margin was located at the Clyde Inlet mouth
823 until ~11.7 ± 2.2 ka (Briner et al., 2005). These results suggest that the ice margin
824 retreated into Clyde Inlet from the bedrock sill at the end of the Younger Dryas.
825 Stabilizations commonly occur at fjord mouths due to the narrowing of the ice stream
826 width, which reduces the ice flux across the grounding line (Åkesson et al., 2018). This
827 stabilization could also be the result of a forced equilibrium in glacial mass balance, where
828 accumulation is too high for the ice sheet margin to retreat into the deeper and narrower
829 fjord but ablation is too high to allow a readvance onto the shelf and the open sea (Syvitski
830 and Shaw, 1995).

831 *5.1.3. Episodic early Holocene retreat in the fjord*

832 The multibeam bathymetry imagery and acoustic sub-bottom profiles show series
833 of moraine systems along the fjord, indicating a step-wise retreat of the LIS margin in the
834 early Holocene, punctuated by intervening periods of fast retreat (Fig. 10e). Two
835 continental moraine ridges located 10 km and 25 km up-fjord from Ailsa Island yielded
836 cosmogenic exposure ages of 11.2 ± 1.2 and 10.0 ± 1.5 ka, respectively (Briner et al.,
837 2007). These ages represent minimum ages for the deglaciation and are probably coeval
838 or younger than the outer fjord moraine (GL6).

839 Few ages are available in the middle section of Clyde Inlet. However, basal ages
840 collected in three lakes near the adjacent Inugsuin Fjord constrain the deglaciation of the

841 middle section to ~10.5 ka cal. BP (Thomas et al., 2010). Ice retreat was probably more
842 or less synchronous in Clyde Inlet, as the continental moraine ridges in the outer fjord
843 yield slightly older ages and a bedrock sample from an unnamed island yielded a
844 cosmogenic exposure age of 10.2 ± 2.2 ka (Briner et al., 2007). Furthermore, cosmogenic
845 dating in Naqsaq Valley indicate alpine glacier stabilization and moraine deposition at
846 ~10.2 ± 0.2 ka (Young et al., 2021). It is therefore possible that the middle fjord moraines
847 (GL7 and GL8) were deposited around that time.

848 During the Cockburn substage, multiple moraines were deposited in the inner
849 fjord and at the fjord head (Fig. 10f). Wood and shell samples collected in a tributary
850 valley 40 km upstream from the fjord head by Briner et al. (2007) yielded identical ages
851 of ~9.3 ka cal. BP for deglaciation of the inner fjord. These ages are in agreement with
852 new basal ages from sediment cores GeoB22348-3 and GeoB22346-3 (Fig. 9), which in
853 turn are constraining the timing of the inner fjord moraines (GL9-GL11) between 9.4 and
854 8.8 ka cal. BP. Similarly, radiocarbon ages from shells collected in deltas at the head of
855 Clyde Inlet indicate that the ice margin retreated beyond the fjord head between 9.1 and
856 8.6 ka cal. BP (Briner et al., 2007). Similar ages from adjacent Inugsuin Fjord and Sam
857 Ford Fjord corroborate these observations (Andrews and Drapier, 1967; Briner et al.,
858 2009a; Syvitski et al., 2022). An ice-contact delta located at the fjord head yielded
859 cosmogenic exposure age of ~8.3 ka ± 0.3 ka (Briner et al., 2007; Young et al., 2013).
860 Radiocarbon ages collected 4 km upstream of the ice-contact delta yielded an age of ~7.9
861 ka cal. BP for the deglaciation of the fjord head (Briner et al., 2007). Deglaciation of the
862 fjord head is marked by a steep decline in Ca/Ti, corresponding to a decrease in coarser
863 sediment input from the ice margin directly into the fjord. The age of ~7.9 ka cal. BP is
864 also in agreement with the shell sample from core GeoB22346-3 indicating that ice had
865 retreated from the fjord head before 6.2 ka cal. BP.

866 The results from Clyde Inlet notably contrast with models previously proposed
867 from eastern Baffin Island, where the LIS was believed to have retreated in a catastrophic
868 pattern along the fjords (Briner et al., 2007, 2009a). Alternatively, the results support a
869 more episodic deglaciation model with multiple ice margin stabilizations and moraine
870 formation proposed for fjords of northeastern Baffin Islands (Brouard and Lajeunesse,
871 2019a).

872 Subsequently to the withdrawal of its ice margin from Clyde Inlet (Fig. 10g), the
873 LIS began a slow retreat towards the south until the Barnes Ice Cap became isolated
874 (Miller et al., 2005; Briner et al., 2009). The LIS and local glaciers receded beyond their
875 current position until the onset of the Neoglacial ~4.5 ka BP (Miller et al., 2005; Young
876 et al., 2015). During that period, cooler climatic conditions prevailed and local glaciers
877 readvanced into the fjord, as marked by lateral moraines from tributary valleys and
878 glaciofluvial fans (Fig. 6A-B). Rapidly deposited layers are identified in cores of the inner
879 fjord and are marked by sharp peaks in Ca/Ti ratios and could relate to these readvances.
880 These coarse layers could also either represent increased sediment input by glacial
881 meltwater or deposits by glacier-lake outburst floods caused by the oscillation of the
882 Barnes Ice Cap repeatedly blocking the Clyde River outlet (Barnett and Holdsworth,
883 1974; Andrews and Barnett, 1979).

884 **5.2. Controls on stabilizations and variability of ice retreat**

885 Several external (e.g., atmospheric temperatures, changes in sea level and ocean-
886 driven melting) and local factors (e.g., topography and bathymetry) have possibly
887 asserted a certain control on the deglaciation patterns in the Clyde fjord-cross-shelf trough
888 system. Comparing the chronology presented in the previous section to a compilation of
889 climatic records allows establishing correlations between the deglaciation and potential
890 factors that may have influenced retreat of the ice margin across the system (Fig 11).

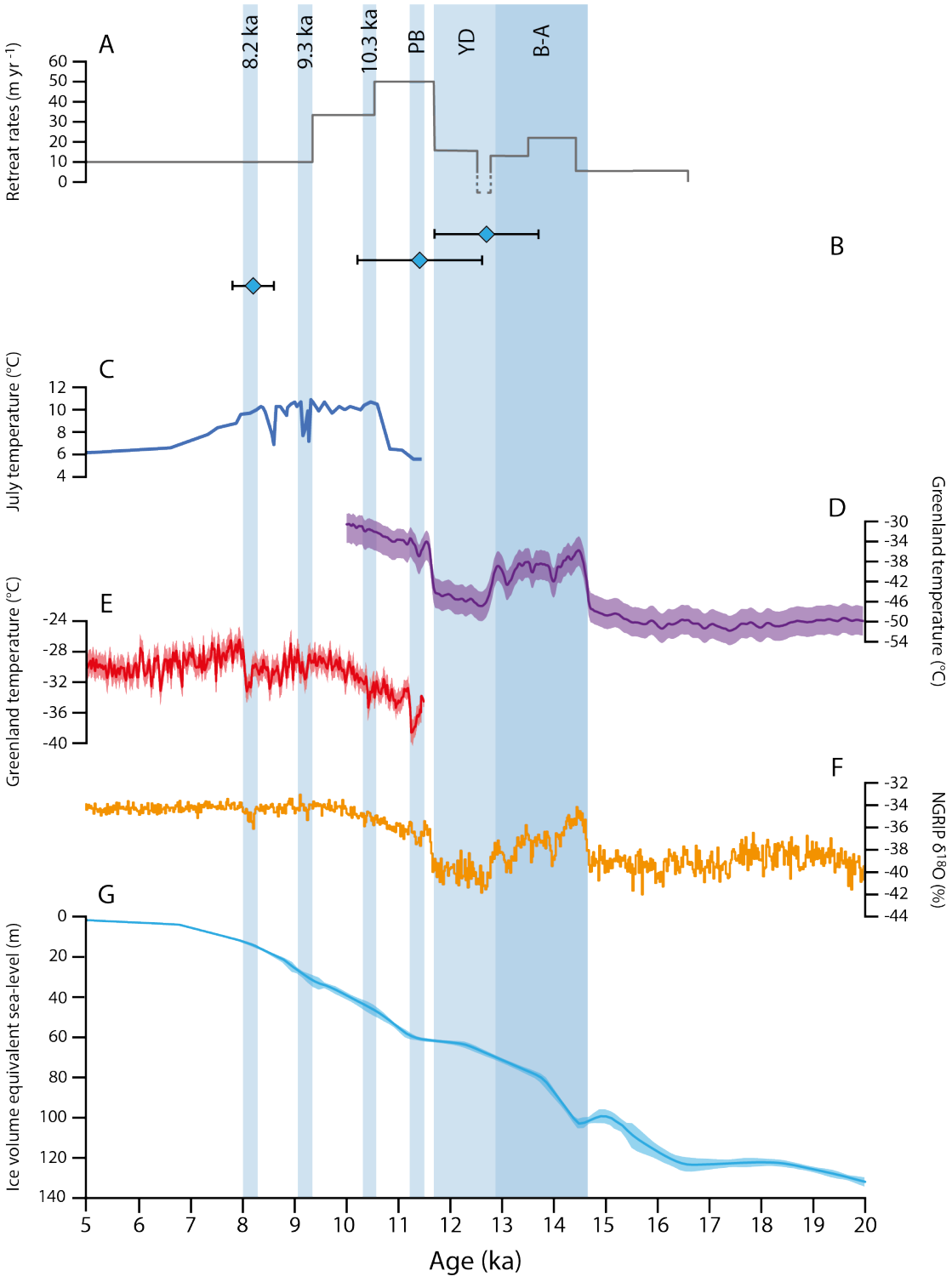

Figure 11 (A) Average retreat rates between stabilizations in the Clyde fjord-cross-shelf trough system. The dashed line represents the uncertainties regarding the length and magnitude of the ice margin readvance during the Younger Dryas. (B) Exposure ages of moraine ridges along Clyde Inlet from Briner et al. (2007), recalculated using the Baffin Bay production rate (Young et al., 2013). (C) Chironomid-derived July temperature reconstruction from Lake CF8, eastern Baffin Island (dark blue; Axford et al., 2009). (D) Greenland mean-annual temperatures reconstructed using gas-phase δ15N-N2 measurements (purple - ±1σ; Buizert et al., 2014). (E) Greenland mean-annual temperatures reconstructed using gas-phase δAr-N2 measurements (red - ±2σ; Kobashi et al., 2017). (F) δ18O record from NGRIP project (orange; Rasmussen et al., 2014). (G) Ice volume equivalent sea-level (blue - ±1σ; Lambeck et al., 2014). Vertical bars represent cold and warm intervals discussed in the text. B-A: Bølling–Allerød; YD: Younger Dryas; PB: Preboreal.

902 *5.2.1. External forcing as the principal driver of ice retreat patterns*

903 The temporal framework presented in the previous section suggest that climate
904 played a dominant role in driving first-order deglaciation patterns in Clyde Inlet, as ice
905 retreat coincides with periods of warming climate and stabilizations are synchronous with
906 cooling events (Fig. 11). In turn, sea level changes and oceanic forcing might also have
907 influenced the retreat rates of the ice margin along the Clyde fjord-cross-shelf trough
908 system (Fig. 11).

909 Rapidly rising sea-level (>40 mm/year; Lambeck et al., 2014) probably favored
910 the initial collapse of the Clyde ice shelf and rapid retreat of the CIS in the early phases
911 of the deglaciation (Couette et al., 2022). Changes in the eustatic level may have provoked
912 the lift-off of the local ice shelf, increasing the area of the ice margin in contact with the
913 water column, making it more vulnerable to ocean forcings (Joughin et al., 2012;
914 Jamieson et al., 2014; Jennings et al., 2018). The global sea-level rise initiated at ~16.5
915 ka eventually led to the ice front destabilization, which induced rapid retreat of the ice
916 margin (~25 m/year). Rapidly rising global sea level has been speculated to have triggered
917 the collapse and/or rapid retreat of marine-based ice sheets in the Northern Hemisphere
918 following the LGM (e.g., Winsborrow et al., 2010; Jakobsson et al., 2011; Rydningen et
919 al., 2013; Hogan et al., 2016; Arndt et al., 2017; Callard et al., 2018). In turn, the timing
920 of ice-margin retreat from outer Clyde Trough is synchronous with the onset of the
921 Bølling–Allerød interstadial (~14.5 – 12.9 ka BP), a period of globally warmer
922 temperatures (Rasmussen et al., 2014). It also coincides with extensive ice mass loss
923 around Baffin Bay, as ice streams were retreating from the outer shelf in Western
924 Greenland (i.e., Sheldon et al., 2016; Jennings et al., 2017) and large numbers of icebergs
925 were released from northern Baffin Bay (i.e., Andrews et al., 1998; Simon et al., 2012;
926 Jackson et al., 2017). Reduced global sea level rise during the second half of the Bølling–

Allerød (~12 mm/year – Lambeck et al., 2014) probably contributed to a slow-down of the ice-margin retreat in Clyde Trough (~12.5 m/year). However, lower rates of sea level rise alone do not explain the slower deglaciation pattern, as it was not observed in neighbouring troughs (Brouard and Lajeunesse, 2017).

The beginning of the Younger Dryas (~12.9 – 11.7 ka BP) was regionally marked by an abrupt lowering of the temperature by 2°C (Rasmussen et al., 2014). This sudden decrease in temperature likely favoured a readvance of the LIS margin, before resuming its slow retreat as the temperature gradually increased again. The presence of the moraine indicating stagnation at the fjord mouth is consistent with the relatively cold conditions across Baffin Bay at the end of the Younger Dryas (Buizert et al., 2014; Rasmussen et al., 2014) that promoted a positive mass balance and possibly counteracted ice loss by calving at the ice margin.

Alternatively, the early Holocene was marked by warmer atmospheric temperature around the Baffin Bay region, which favoured extensive ice margin retreat (Pendleton et al., 2019; Lesnek et al., 2020). While temperatures were generally warm during the Holocene, cold spells were recorded in different proxies (i.e., Axford et al., 2009; Rasmussen et al., 2014) and appear to have favored ice margin stabilizations in Clyde Inlet. This deglaciation model is in agreement with observations around Baffin Bay where widespread moraine deposition have been associated with cold-climate oscillations at 11.3, 10.4, 9.3 and 8.2 ka (Young et al., 2020; Lesnek et al., 2020).

Inflow of subsurface water might have been an additional contributor to retreat rates in our study area through deglaciation. The intrusion of subsurface warm water have provoked accelerated melting and enhanced ice-margin retreat in modern-day marine-terminating glaciers (e.g., Straneo et al., 2011; Jeong et al., 2016; Howe et al., 2019), as

well as on the shelves and fjords of many formerly glaciated regions (e.g., Sheldon et al., 2016; Arndt et al., 2017; Batchelor et al., 2019a; Allaart et al., 2020). However, the Baffin Island Current incorporates colder Arctic water from the CAA and Nares Strait (Tang et al., 2004; Münchow et al., 2015), therefore lowering the layer of warmer subsurface water. A reduction in the depth of warmer currents would weaken its influence on ice retreat along the Baffin shelf, in particular for the shallower Clyde Trough. Moreover, the shallow fjord-mouth sill (< 200 m) probably prevented subsurface warm water from entering the fjord and triggering a catastrophic retreat. It is therefore unlikely that inflow of warmer currents had major influence on the retreat of the CIS.

Although external forcing played an unequivocal role in the deglaciation of Clyde Inlet, the variability in retreat patterns when compared to other neighbouring fjord-cross-shelf trough systems indicates a local control on LIS margin oscillations.

5.2.2. Fjord/trough geometry controlling ice margin stabilization

Local-scale topography appears to have been a key factor in controlling the location of stabilizations during the retreat of the CIS. Depositional wedges and related stabilizations have been noted where topographic constrictions, highs and/or bends in the trough orientation occur. Although most topographic controls in the trough are bedrock-influenced, older GZWs might have produced a pinning point adequate enough to help the ice margin stabilize in the outer trough at the LGM (Fig. 7). Acting as a topographic high, these older GZWs restrained the LIS from flowing farther seaward regardless of the wider diffluent bed morphology by increasing the basal drag exerted on the ice stream (Dowdeswell and Fugelli, 2012; Batchelor and Dowdeswell, 2015; Hogan et al., 2016; Bart et al., 2017; Danielson and Bart, 2019; Greenwood et al., 2021; Ottesen et al., 2022). A bend in the trough orientation, corresponding to a change in bedrock lithology, possibly further contributed to the formation of the morainal bank by enhancing lateral drag on the

side of the glacier (Syvitski and Shaw, 1995; Lyså and Vorren, 1997; Laberg et al., 2009; Jamieson et al., 2012, 2014; Ó Cofaigh et al., 2014; Bradwell et al., 2019). The relatively shallower depths compared to other cross-shelf trough systems of northeastern Baffin Island probably restricted the area of the ice front in contact with the ocean, resulting in a slower deglaciation in the middle trough as observed in similar settings (Arndt et al., 2017; Jakobsen et al., 2020). The shallower depths likely also contributed to the slower deglaciation pattern observed across the retrograde slope of the mid- and inner trough following the YD readvance.

In contrast, deeper water in the fjord may have favored the acceleration in ice retreat (>50 m/year). Loss of contact with vertical pinning point reduces drag which, in turn, increases mass flow and iceberg calving rates (Syvitski and Shaw, 1995; Jamieson et al., 2014; Batchelor et al., 2019a). Coupled with the generally warmer atmosphere temperature of the early Holocene, it created an ideal setting for an enhanced retreat rate of the LIS in Clyde Inlet. However, cold events probably provoked intervening stabilizations of the ice margin in Clyde Inlet, while the fjord geometry influenced the location of most stabilizations. The outer fjord moraine is located at a pinning point created by multiple islands at the confluence of Clyde Inlet and Inugsuin Fjord. This pinning-point allowed the ice margin to anchor and stabilize on the topographic high between islands. The location of the middle fjord moraine at the confluence of Clyde Inlet and Cormack Arm suggests, however, the influence of a funnel-shaped constriction of the ice (i.e., Syvitski and Shaw, 1995; Brouard and Lajeunesse, 2019a). Other ice-margin stabilizations in the inner fjord occurred at bends and lateral constrictions of the fjord width because of enhanced lateral-drag (Jamieson et al., 2012; Åkesson et al., 2018; Batchelor et al., 2019a; Brouard and Lajeunesse, 2019a). It must be emphasized here that

not all constrictions or bends are associated with a stabilization in the fjord, as climate is likely the main driver for initiating a slow-down of the ice retreat.

6. Conclusions

The combination of multibeam bathymetry imagery, seismostratigraphic profiles and sediment cores collected in the Clyde Inlet fjord-cross-shelf trough system (NE Baffin Island) provide new insights into the extent and retreat patterns of the Laurentide Ice Sheet margin in the region during the Last Glacial cycle. Key results of this analysis are:

- The LIS margin probably did not extend all the way across the continental shelf in Clyde Trough during the LGM; its maximal extent was rather located some 10 km from the shelf break. However, as the absence of direct dating on the upper continental slope restrains us from providing confirmation, the question of the maximal extent of the LIS in Clyde Trough remains open.
- Deglaciation on the shelf was temporally constrained to the late glacial (16-11.7 ka). It was marked by an initial collapse of the Clyde ice shelf and rapid LIS margin retreat, followed by a slow retreat of the ice margin with intervening stabilizations interrupted by a readvance during the Younger Dryas. This deglaciation pattern differs from observations made in other troughs of northeastern Baffin Island shelf, where it appears to have been more rapid and episodic with wider spaced GZWs.
- Similarly to other fjords of northeastern Baffin Island, the ice margin retreated into Clyde Inlet in a less catastrophic pattern than previously proposed for the early Holocene (11.7-8 ka). Our age constraints support earlier works that suggest numerous ice margin stabilizations during the early Holocene, which could be linked

to cold climate events at ~10.3, ~9.3 and ~8.2 ka. The retreat was, however, rapid between successive stabilizations due to greater water depths in the fjord.

- Climate was the main driver of deglaciation in the Clyde area, as the available chronology suggests that most stabilizations coincided with regional-wide cooling events. Deglaciation patterns in the Clyde area were strongly influenced by topography, as ice margin stabilizations occurred at pinning points in both the trough and fjord. Oceanic forcing, such as global sea level fluctuations and ocean temperatures, appears to only have a secondary influence on rates of ice sheet retreat in the Clyde fjord-cross-shelf trough system.

These results highlight the variability of ice-sheet retreat patterns and controls along a single high Arctic fjord-cross-shelf trough system, and from one system to another. However, uncertainties remain concerning the timing of ice margin stabilizations on northeastern Baffin Island, especially on the continental shelf. Future work on Baffin Island fjord-cross-shelf trough systems should therefore focus on establishing a robust deglaciation chronology combining both marine- and terrestrial-based investigations, which would improve knowledge on factors controlling glacier behaviour and provide key information for testing numerical simulations on climate and predicting future ice mass loss in a warming world.

Data availability

The multibeam bathymetric data collected in 2017 during expedition MSM66 have been deposited in the PANGAEA repository (https://doi.org/10.1594/PANGAEA.902341). The multibeam bathymetric data from ArcticNet cruises can be visualized on the Université Laval Géoindex + website (http://geoindex-plus.bibl.ulaval.ca). The Parasound profiles collected in 2017 during expedition MSM66 have been deposited in

the PANGAEA repository (https://doi.pangaea.de/10.1594/PANGAEA.944843). The seismic reflection data along with the acquisition specifics are available on the Marine Data Holding public repository of National Resources Canada (http://geogratis.gc.ca/).

Author contributions

POC conceived the study and initiated this project in cooperation with PL and JFG. POC interpreted the geophysical data sets, conducted the sediment core analysis, wrote the paper and prepared the figures. PL, JFG, BD, CG, DH, and EB were involved in the discussion of the data and contributed to the final version of this paper.

Acknowledgments

We are thankful to the captains, crews and scientific participants on the different cruises for their help and support during the expeditions. This project was funded by the *ArcticNet Network of Centers of Excellence, Natural Sciences and Engineering Research Council of Canada* (NSERC) and *Sentinelle Nord (Apogée Canada)* grants to PL, the *Deutsche Forschungsgemeinschaft* (DFG) grants to BD, CG and DH for ship-time and to DH for the International Research Training Group "*ArcTrain*" (IRTG 1904), as well as Université de Strasbourg grants to POC. We are grateful to *ArcTrain Canada* for providing financial support to this project. This study was supported by *Fonds québécois de la recherche sur la nature et les technologies* (FRQNT) through a travel grant to POC allowing sediment core analysis at the Center for Marine Environmental Sciences (MARUM – University of Bremen). We also thank Jens Weiser and Thomas Westerhold for their help with laboratory work. This paper was greatly improved by detailed and constructive comments by O. Bourgeois, C. Ó Cofaigh and D. B. Praeg, as well as formal reviews by E. L. King, one anonymous reviewer and the handling editor Antje Voelker.

References

Aarseth, I., Austbø, P. K., Risnes, H., 1997. Seismic stratigraphy of Younger Dryas ice-marginal deposits in western Norwegian fjords. Norsk Geologisk Tidsskrift 77(2), 65-85.

Åkesson, H., Nisancioglu, K. H., Nick, F. M., 2018. Impact of fjord geometry on grounding line stability. Frontiers in Earth Science 71, 1-16.

Allaart, L., Müller, J., Schomacker, A., Rydningen, T. A., Håkansson, L., Kjellman, S. E., Mollenhauer, G., Forwick, M., 2020. Late Quaternary glacier and sea-ice history of northern Wijdefjorden, Svalbard. Boreas 49(3), 417-437.

Andrews, J. T., Drapier, L., 1967. Radiocarbon dates obtained through Geographical Branch field observations. Geographical Bulletin 9(2), 115-62.

Andrews, J. T., Ives, J. D., 1978. "Cockburn" Nomenclature and the Late Quaternary History of the Eastern Canadian Arctic. Arctic and Alpine Research 10(3), 617-633.

Andrews, J. T., Barnett, D., 1979. Holocene (Neoglacial) moraine and proglacial lake chronology, Barnes ice cap, Canada. Boreas 8(3), 341-358.

Andrews, J. T., Kirby, M. E., Aksu, A., Barber, D. C., Meese, D., 1998. Late Quaternary detrital carbonate (DC-) layers in Baffin Bay marine sediments (67°–74° N): correlation with Heinrich events in the North Atlantic? Quaternary Science Reviews 17(12), 1125-1137.

Andrews, J.T., Dyke, A.S., 2007. Glaciations: late quaternary in North America. In: Elias, S.A. (Ed.), Encyclopedia of Quaternary Science. Elsevier, Amsterdam, 1095-1101.

Arndt, J. E., Jokat, W., Dorschel, B., 2017. The last glaciation and deglaciation of the Northeast Greenland continental shelf revealed by hydro-acoustic data. Quaternary

1093 Science Reviews 160, 45-56.

1094 Arosio, R., Dove, D., Cofaigh, C. Ó., Howe, J. A. (2018). Submarine deglacial sediment
1095 and geomorphological record of southwestern Scotland after the Last Glacial
1096 Maximum. Marine Geology 403, 62-79.

1097 Axford, Y., Briner, J. P., Cooke, C. A., Francis, D. R., Michelutti, N., Miller, G. H., Smol,
1098 J. P., Thomas, E. K., Wilson, C. R., Wolfe, A. P., 2009. Recent changes in a remote
1099 Arctic lake are unique within the past 200,000 years. Proceedings of the National
1100 Academy of Sciences 106(44), 18443-18446.

1101 Barnett, D. M., Holdsworth, G., 1974. Origin, Morphology, and Chronology of
1102 Sublacustrine Moraines, Generator Lake Baffin Island, Northwest Territories,
1103 Canada. Canadian Journal of Earth Sciences 11(3), 380-408.

1104 Bart, P. J., Anderson, J. B., Nitsche, F., 2017. Post-LGM Grounding-Line Positions of
1105 the Bindschadler Paleo Ice Stream in the Ross Sea Embayment, Antarctica. Journal
1106 of Geophysical Research: Earth Surface 122(10), 1827-1844.

1107 Batchelor, C. L., Dowdeswell, J. A., 2015. Ice-sheet grounding-zone wedges (GZWs) on
1108 high-latitude continental margins. Marine Geology 363, 65-92.

1109 Batchelor, C. L., Dowdeswell, J. A., 2016. Lateral shear-moraines and lateral marginal-
1110 moraines of palaeo-ice streams. Quaternary Science Reviews 151, 1-26.

1111 Batchelor, C. L., Dowdeswell, J. A., Rignot, E., 2018. Submarine landforms reveal
1112 varying rates and styles of deglaciation in North-West Greenland fjords. Marine
1113 Geology 402, 60-80.

1114 Batchelor, C. L., Dowdeswell, J. A., Rignot, E., Millan, R., 2019a. Submarine moraines
1115 in Southeast Greenland fjords reveal contrasting outlet-glacier behaviour since the

Last Glacial Maximum. Geophysical Research Letters 46, 3279–3286.

Batchelor, C. L., Margold, M., Krapp, M., Murton, D. K., Dalton, A. S., Gibbard, P. L.,Stokes, C. R., Murton, J. B., Manica, A., 2019b. The configuration of Northern Hemisphere ice sheets through the Quaternary. Nature Communications 10(1), 1-10.

Bjarnadóttir, L. R., Rüther, D. C., Winsborrow, M., Andreassen, K., 2012. Grounding-line dynamics during the last deglaciation of Kveithola, W Barents Sea, as revealed by seabed geomorphology and shallow seismic stratigraphy. Boreas 42(1), 84-107.

Boulton, G. S., 1986. Push-moraines and glacier-contact fans in marine and terrestrial environments. Sedimentology 33(5), 677-698.

Bradwell, T., Small, D., Fabel, D., Smedley, R. K., Clark, C. D., Saher, M. H., Callard, S. L., Chiverrell, R. C., Dove, C., Moreton, S. G., Roberts, D. H., Duller, G. A. T., Ó Cofaigh, C., 2019. Ice-stream demise dynamically conditioned by trough shape and bed strength. Science Advances 5(4), eaau1380.

Briner, J.P., Miller, G.H., Davis, P.T., Finkel, R.C., 2005. Cosmogenic exposure dating in arctic glacial landscapes: implications for the glacial history of northeastern Baffin Island, Arctic Canada. Canadian Journal of Earth Sciences 42, 67–84.

Briner, J. P., Miller, G. H., Davis, P. T., Finkel, R. C., 2006. Cosmogenic radionuclides from fiord landscapes support differential erosion by overriding ice sheets. Geological Society of America Bulletin 118, 406-420.

Briner, J.P., Overeem, I., Miller, G.H., Finkel, R.C., 2007. The deglaciation of Clyde Inlet, northeastern Baffin Island, Arctic Canada. Journal of Quaternary Science 22, 223–232.

Briner, J.P., Bini, A.C., Anderson, R.S., 2009a. Rapid early Holocene retreat of a

1139 Laurentide outlet glacier through an Arctic fjord. Nature Geoscience 2, 496–499.

1140 Briner, J. P., Davis, P. T., Miller, G. H., 2009b. Latest Pleistocene and Holocene
1141 glaciation of Baffin Island, Arctic Canada: key patterns and chronologies.
1142 Quaternary Science Reviews 28(21-22), 2075-2087.

1143 Briner, J. P., Cuzzone, J. K., Badgeley, Young, N. E., Steig, E. J., Morlighem, M.,
1144 Schlegel, N. J., Hakim, G. J., Schaefer, J. M., Johnson, J. V., Lesnek, A. J., Thomas,
1145 E. K., J., Allan, E., Bennike, O., Cluett, A., Csatho, B., de Vernal, A., Downs, J.,
1146 Larour, E., Nowicki, S., 2020. Rate of mass loss from the Greenland Ice Sheet will
1147 exceed Holocene values this century. Nature 586(7827), 70-74.

1148 Brouard, E., Lajeunesse, P, 2017. Maximum extent and decay of the Laurentide Ice Sheet
1149 in Western Baffin Bay during the Last glacial episode. Scientific Reports 7(1),
1150 10711.

1151 Brouard, E., Lajeunesse, P., 2019a. Glacial to postglacial submarine landform
1152 assemblages in fiords of northeastern Baffin Island. Geomorphology 330, 40-56.

1153 Brouard, E., Lajeunesse, P., 2019b. Submarine geomorphology of the northeastern Baffin
1154 Island fiords and cross-shelf troughs. Journal of Maps 15, 662-676.

1155 Brouard, E., Lajeunesse, P., 2019c. Ice-stream flow switching by up-ice propagation of
1156 instabilities along glacial marginal troughs. The Cryosphere 13(3), 981-996.

1157 Buizert, C., Gkinis, V., Severinghaus, J. P., He, F., Lecavalier, B. S., Kindler, P.,
1158 Leuenberger, M., Carlson, A. E., Vinther, B., Masson-Delmotte, V., White, J. W.
1159 C., Liu, Z., Otto-Bliesner, B., Brook, E. J., 2014. Greenland temperature response to
1160 climate forcing during the last deglaciation. Science 345(6201), 1177-1180.

1161 Callard, S. L., Ó Cofaigh, C., Benetti, S., Chiverrell, R., C., Van Landeghem, K. J. J.,

Saher, M. H., Gales, J. A., Small, D., Clark, C. D., Livingstone, S. J., Fabel, D., Moreton, S. G., 2018. Extent and retreat history of the Barra Fan Ice Stream offshore western Scotland and northern Ireland during the last glaciation. Quaternary Science Reviews 201, 280-302.

Callard, S. L., Cofaigh, C. Ó., Benetti, S., Chiverrell, R. C., Van Landeghem, K. J., Saher, M. H., Livingstone, S. J., Clark, C. D., Fabel, D., Moreton, S. G., 2020). Oscillating retreat of the last British-Irish Ice Sheet on the continental shelf offshore Galway Bay, western Ireland. Marine Geology 420, 106087.

Carlson, A. E., 2009. Geochemical constraints on the Laurentide Ice Sheet contribution to meltwater pulse 1A. Quaternary Science Reviews 28, 1625-1630.

Clark, C. D., 1993. Mega-scale glacial lineations and cross-cutting ice-flow landforms. Earth surface processes and landforms 18(1), 1-29.

Clark, C. D., Tulaczyk, S. M., Stokes, C. R., Canals, M., 2003. A groove-ploughing theory for the production of mega-scale glacial lineations, and implications for ice-stream mechanics. Journal of Glaciology 49(165), 240-256.

Couette, P.-O., Lajeunesse, P., Ghienne, J.-F., Dorschel, B., Gebhardt, C., Hebbeln, D., Brouard, E., 2022. Evidence for an extensive ice shelf in northern Baffin Bay during the Last Glacial Maximum. Communications Earth and Environment 3(1), 1-12.

Dalton, A.S., Margold, M., Stokes, C.R., Tarasov, L., Dyke, A.S., Adams, R.S., Allard, S., Arends, H.E., Atkinson, N., Attig, J.W., Barnett, P.J., Barnett, R.L., Batterson, M., Bernatchez, P., Borns, H.W., Breckenridge, A., Briner, J.P., Brouard, E., Campbell, J.E., Carlson, A.E., Clague, J.J., Curry, B.B., Daigneault, R.A., Dubé-Loubert, H., Easterbrook, D.J., Franzi, D.A., Friedrich, H.G., Funder, S., Gauthier, M.S., Gowan, A.S., Harris, K.L., Hétu, B., Hooyer, T.S., Jennings, C.E., Johnson,

M.D., Kehew, A.E., Kelley, S.E., Kerr, D., King, E.L., Kjeldsen, K.K., Knaeble, A.R., Lajeunesse, P., Lakeman, T.R., Lamothe, M., Larson, P., Lavoie, M., Loope, H.M., Lowell, T.V., Lusardi, B.A., Manz, L., McMartin, I., Nixon, F.C., Occhietti, S., Parkhill, M.A., Piper, D.J.W., Pronk, A.G., Richard, P.J.H., Ridge, J.C., Ross, M., Roy, M., Seaman, A., Shaw, J., Stea, R.R., Teller, J.T., Thompson, W.B., Thorleifson, L.H., Utting, D.J., Veillette, J.J., Ward, B.C., Weddle, T.K., Wright, H.E., 2020. An updated radiocarbon-based ice margin chronology for the last deglaciation of the North American Ice Sheet Complex. Quaternary Science Reviews 234, 106223.

Danielson, M., Bart, P. J., 2019. Topographic control on the post-LGM grounding zone locations of the West Antarctic Ice Sheet in the Whales Deep Basin, Eastern Ross Sea. Marine Geology 407, 248-260.

Davis, P. T., Briner, J. P., Coulthard, R. D., Finkel, R. W., Miller, G. H., 2006. Preservation of Arctic landscapes overridden by cold-based ice sheets. Quaternary Research 65, 156-163.

De Angelis, H., Kleman, J., 2007. Palaeo-ice streams in the Foxe/Baffin sector of the Laurentide Ice Sheet. Quaternary Science Reviews 26, 1313–1331.

Dorschel B., Allan, E., Bartels, M., Campbell, C., Couette. P. O., Diekamp, V., Dreutter, S., Duboc, Q., Geils, J., Greco, M., Lenz, K. F., Lübben, B., Lütjens, M., Madaj, L., Perez, L., Recinos, B., Saini, J., Schade, T., Täuber, F., Ulner, L. C., Warnke, F., Weiser, J., 2017. WESTBAFF Reconstruction of the Laurentide Ice sheet drainage into the northwest Baffin Bay and the palaoceanography of the west Baffin Bay - Cruise No. MSM66 - July 22 - August 28, 2017 - Nuuk (Greenland) - Reykjavik (Iceland), Maria S. Merian Berichte, Gutachterpanel Forschungsschiffe, Bonn, 52 p.

1210 Dowdeswell, J.A., Whittington, R.J., Marienfeld, P., 1994. The origin of massive
1211 diamicton facies by iceberg rafting and scouring, Scoresby Sund, East Greenland.
1212 Sedimentology 41, 21-35.

1213 Dowdeswell, J. A., Whittington, R. J., Jennings, A. E., Andrews, J. T., Mackensen, A.,
1214 Marienfeld, P., 2000. An origin for laminated glacimarine sediments through sea-
1215 ice build-up and suppressed iceberg rafting. Sedimentology 47, 557-576.

1216 Dowdeswell, J. A., Ottesen, D., Evans, J., Cofaigh, C. Ó., Anderson, J. B., 2008.
1217 Submarine glacial landforms and rates of ice-stream collapse. Geology 36(10), 819-
1218 822.

1219 Dowdeswell, J. A., Fugelli, E. M. G., 2012. The seismic architecture and geometry of
1220 grounding-zone wedges formed at the marine margins of past ice sheets. Geological
1221 Society of America Bulletin 124(11-12), 1750-1761.

1222 Dowdeswell, J. A., Vásquez, M., 2013. Submarine landforms in the fjords of southern
1223 Chile: implications for glacimarine processes and sedimentation in a mild glacier-
1224 influenced environment. Quaternary Science Reviews 64, 1-19.

1225 Dowdeswell, J. A., Hogan, K. A., Cofaigh, C. Ó., Fugelli, E. M. G., Evans, J., Noormets,
1226 R., 2014. Late Quaternary ice flow in a West Greenland fjord and cross-shelf trough
1227 system: submarine landforms from Rink Isbrae to Uummannaq shelf and slope.
1228 Quaternary Science Reviews 92, 292-309.

1229 Dowdeswell, J. A., Hogan, K. A., Arnold, N. S., Mugford, R. I., Wells, M., Hirst, J. P. P.,
1230 Decalf, C., 2015. Sediment-rich meltwater plumes and ice-proximal fans at the
1231 margins of modern and ancient tidewater glaciers: Observations and modelling.
1232 Sedimentology 62(6), 1665-1692.

1233 Dowdeswell, J. A., Todd, B. J., Dowdeswell, E. K., Batchelor, C. L., 2016. Ice-sculpted
1234 bedrock in channels of the Canadian Arctic Archipelago. In: Dowdeswell, J. A.,
1235 Canals, M., Jakobsson, M., Todd, B. J., Dowdeswell, E. K., Hogan, K. (Eds.), Atlas
1236 of submarine glacial landforms: modern, Quaternary and ancient. Geological
1237 Society, London, Memoirs 46, 59-60.

1238 Dyke, A. S., Morris, T. F., 1988. Drumlin fields, dispersal trains, and ice streams in Arctic
1239 Canada. Canadian Geographer 32(1), 86-90.

1240 Dyke, A. S., Andrews, J. T., Clark, P. U., England, J. H., Miller, G. H., Shaw, J., Veillette,
1241 J. J., 2002. The Laurentide and Innuitian ice sheets during the Last Glacial
1242 Maximum. Quaternary Science Reviews 21, 9–31.

1243 Dyke, A. S., 2004. An outline of North American deglaciation with emphasis on central
1244 and northern Canada. Developments in Quaternary Sciences 2, 373-424.

1245 Evans, D. J., Rea, B. R., 1999. Geomorphology and sedimentology of surging glaciers: a
1246 land-systems approach. Annals of Glaciology 28, 75-82.

1247 Fader, G.B., Amos, C.L., Best, M.A., Cameron, G.D.M., Jennings, A., Josenhans, H.,
1248 MacLean, B., Powell, C., Sonnichsen, G., 1989. Quaternary geology of the
1249 continental margin of Eastern Canada. Geological Survey of Canada, Map 1705A,
1250 Scale 1:5,000,000.

1251 Favier, L., Durand, G., Cornford, S. L., Gudmundsson, G. H., Gagliardini, O., Gillet-
1252 Chaulet, F., Zwinger, T., Payne, A. J., Le Brocq, A. M., 2014. Retreat of Pine Island
1253 Glacier controlled by marine ice-sheet instability. Nature Climate Change 4(2), 117-
1254 121.

1255 Flink, A. E., Noormets, R., 2018. Submarine glacial landforms and sedimentary

environments in Vaigattbogen, northeastern Spitsbergen. Marine Geology 402, 244-263.

Gilbert, R., Naldrett, D. L., Horvath, V. V., 1990. Holocene sedimentary environment of Cambridge fiord, Baffin Island, northwest Territories. Canadian Journal of Earth Sciences 27, 271-280.

Greenwood, S. L., Simkins, L. M., Winsborrow, M. C., Bjarnadóttir, L. R., 2021. Exceptions to bed-controlled ice sheet flow and retreat from glaciated continental margins worldwide. Science advances 7(3), eabb6291.

Harrison, S., Smith, D. E., Glasser, N. F., 2018. Late Quaternary meltwater pulses and sea level change. Journal of Quaternary Science 34, 1-15.

Heaton, T. J., Köhler, P., Butzin, M., Bard, E., Reimer, R. W., Austin, W. E., Bronk Ramson, C., Grottes, P. M., Hughen, K. A., Kromer, B., Reimer, P. J., Adkins, J., Burke, A., Cook, M. S., Olsen, J., Skinner, L. C., 2020. Marine20—the marine radiocarbon age calibration curve (0–55,000 cal BP). Radiocarbon 62(4), 779-820.

Heaton, T. J., Bard, E., Ramsey, C. B., Butzin, M., Hatté, C., Hughen, K. A., Köhler, P., Reimer, P. J., 2022. A Response to Community Questions on the Marine20 Radiocarbon Age Calibration Curve: Marine Reservoir Ages and the Calibration of 14C samples from the Oceans. Radiocarbon, 1-27.

Hodgson, D. A., Graham, A. G., Griffiths, H. J., Roberts, S. J., Cofaigh, C. Ó., Bentley, M. J., Evans, D. J., 2014. Glacial history of sub-Antarctic South Georgia based on the submarine geomorphology of its fjords. Quaternary Science Reviews 89, 129-147.

Hogan, K. A., Cofaigh, C. Ó., Jennings, A. E., Dowdeswell, J. A., Hiemstra, J. F., 2016.

1279 Deglaciation of a major palaeo-ice stream in Disko Trough, West Greenland.
1280 Quaternary Science Reviews 147, 5-26.

1281 Hogan, K. A., Jakobsson, M., Mayer, L., Reilly, B. T., Jennings, A. E., Stoner, J. S.,
1282 Nielsen, T., Andresen, K. J., Nørmark, Heirman, K. A., Kamla, E., Jerram, K.,
1283 Stranne, C., Mix, A., 2020. Glacial sedimentation, fluxes and erosion rates
1284 associated with ice retreat in Petermann Fjord and Nares Strait, north-west
1285 Greenland. The Cryosphere 14, 261-286.

1286 Howe, J. A., Husum, K., Inall, M. E., Coogan, J., Luckman, A., Arosio, R., Abernethy,
1287 C., Verchili, D., 2019. Autonomous underwater vehicle (AUV) observations of
1288 recent tidewater glacier retreat, western Svalbard. Marine Geology 417, 106009.

1289 Hughes, P. D., Gibbard, P. L., Ehlers, J., 2013. Timing of glaciation during the last glacial
1290 cycle: evaluating the concept of a global 'Last Glacial Maximum'(LGM). Earth-
1291 Science Reviews 125, 171-198.

1292 Jackson, G.D., Blusson, S.L., Crawford, W.J., Davidson, A., Morgan, W.C., Kranck,
1293 E.H., Riley, G., Eade, K.E., 1984, Geology, Clyde River, District of Franklin:
1294 Geological Survey of Canada, "A" Series Map 1582A, scale 1:250,000.

1295 Jackson, R., Carlson, A. E., Hillaire-Marcel, C., Wacker, L., Vogt, C., Kucera, M., 2017.
1296 Asynchronous instability of the North American-Arctic and Greenland ice sheets
1297 during the last deglaciation. Quaternary Science Reviews 164, 140-153.

1298 Jakobsson M., Anderson J. B., Nitsche F. O., Dowdeswell, J. A., Gyllencreutz, R.,
1299 Kirchner, N., Mohammad, R., O'Regan, M., Alley, R. B., Anandakrishnan, S.,
1300 Erikksson, B., Kirshner, A., Fernandez, R., Stolldorf, T., Minzoni, R., Majewski,
1301 W., 2011. Geological record of ice shelf break-up and grounding line retreat, Pine
1302 Island Bay, west Antarctica. Geology 39: 691–694.

Jakobsson, M., Mayer, L., Coakley, B., Dowdeswell, J.A., Forbes, S., Fridman, B., Hodnesdal, H., Noormets, R., Pedersen, R., Rebesco, M., Schenke, H.W., Zarayskaya, Y., Accettella, D., Armstrong, A., Anderson, R.M., Bienhoff, P., Camerlenghi, A., Church, I., Edwards, M., Gardner, J.V., Hall, J.K., Hell, B., Hestvik, O., Kristoffersen, Y., Marcussen, C., Mohammad, R., Mosher, D., Nghiem, S.V., Pedrosa, M.T., Travaglini, P.G., Weatherall, P., 2014. The International Bathymetric Chart of the Arctic Ocean (IBCAO) Version 3.0. Geophysical Research Letters 39 (12), L12609.

Jakobsson, M., Hogan, K. A., Mayer, L. A., Mix, A., Jennings, A., Stoner, J., Eriksson, B., Jerram, K., Mohammad, R., Pearce, C., Reilly, B., Stranne, C., 2018. The Holocene retreat dynamics and stability of Petermann Glacier in northwest Greenland. Nature communications 9(1), 2104.

Jamieson, S. S., Vieli, A., Livingstone, S. J., Cofaigh, C. Ó., Stokes, C., Hillenbrand, C. D., Dowdeswell, J. A., 2012. Ice-stream stability on a reverse bed slope. Nature Geoscience 5(11), 799-802.

Jamieson, S. S., Vieli, A., Cofaigh, C. Ó., Stokes, C. R., Livingstone, S. J., Hillenbrand, C. D., 2014. Understanding controls on rapid ice-stream retreat during the last deglaciation of Marguerite Bay, Antarctica, using a numerical model. Journal of Geophysical Research: Earth Surface 119(2), 247-263.

Jenner, K. A., Campbell, D. C., Piper, D. J. W., 2018. Along-slope variations in sediment lithofacies and depositional processes since the Last Glacial Maximum on the northeast Baffin margin, Canada. Marine Geology 405, 92-107.

Jennings, A. E., 1993. The Quaternary history of Cumberland Sound, southeastern Baffin Island: the marine evidence. Géographie physique et Quaternaire 47(1), 21-42.

Jennings, A. E., Sheldon, C., Cronin, T. M., Francus, P., Stoner, J., Andrews, J., 2011. The Holocene history of Nares Strait: Transition from glacial bay to Arctic-Atlantic throughflow. Oceanography 24, 26-41.

1330 Jennings, A. E., Walton, M. E., Ó Cofaigh, C. O. L. M., Kilfeather, A., Andrews, J. T.,
1331 Ortiz, J. D., de Vernal, A., Dowdeswell, J. A., 2014. Paleoenvironments during
1332 Younger Dryas-E arly Holocene retreat of the Greenland Ice Sheet from outer Disko
1333 Trough, central west Greenland. Journal of Quaternary Science 29(1), 27-40.

1334 Jennings, A. E., Andrews, J. T., Cofaigh, C. Ó., Onge, G. S., Sheldon, C., Belt, S. T.,
1335 Cabedo-Sanz, P., Hillaire-Marcel, C., 2017. Ocean forcing of Ice Sheet retreat in
1336 central west Greenland from LGM to the early Holocene. Earth and Planetary
1337 Science Letters 472, 1-13.

1338 Jennings, A. E., Andrews, J. T., Cofaigh, C. Ó., St-Onge, G., Belt, S., Cabedo-Sanz, P.,
1339 Pearce, C., Hillaire-Marcel, C., Campbell, D. C., 2018. Baffin Bay
1340 paleoenvironments in the LGM and HS1: Resolving the ice-shelf question. Marine
1341 Geology 402, 5-16.

1342 Jeong, S., Howat, I. M., Bassis, J. N., 2016. Accelerated ice shelf rifting and retreat at
1343 Pine Island Glacier, West Antarctica. Geophysical Research Letters 43(22), 11-720.

1344 Joughin, I., Alley, R. B., Holland, D. M., 2012. Ice-sheet response to oceanic forcing.
1345 science 338(6111), 1172-1176.

1346 King, L. H., 1976. Relict iceberg furrows on the Laurentian Channel and western Grand
1347 Banks. Canadian Journal of Earth Sciences 13(8), 1082-1092.

1348 King, E. L., Haflidason, H., Sejrup, H. P., Løvlie, R., 1998. Glacigenic debris flows on
1349 the North Sea Trough Mouth Fan during ice stream maxima. Marine Geology 152(1-
1350 3), 217-246.

1351 Kleman, J., Jansson, K., De Angelis, H., Stroeven, A.P., Hattestrand, C., Alm, G., Glasser,
1352 N.F., 2010. North American Ice Sheet build-up during the last glacial cycle, 115-21

kyr. Quaternary Science Reviews 29, 17-18.

Laberg, J. S., Eilertsen, R. S., Vorren, T. O., 2009. The paleo–ice stream in Vestfjorden, north Norway, over the last 35 ky: Glacial erosion and sediment yield. Geological Society of America Bulletin 121(3-4), 434-447.

Lajeunesse, P., Dietrich, P., Ghienne, J. F., 2019. Late Wisconsinan grounding zones of the Laurentide Ice Sheet margin off the Québec North Shore (NW Gulf of St Lawrence). Geological Society, London, Special Publications 475(1), 241-259.

Lambeck, K., Rouby, H., Purcell, A., Sun, Y., Sambridge, M., 2014. Sea level and global ice volumes from the Last Glacial Maximum to the Holocene. Proceedings of the National Academy of Sciences 111(43), 15296-15303.

Lesnek, A. J., Briner, J. P., Young, N. E., Cuzzone, J. K., 2020. Maximum southwest Greenland Ice Sheet recession in the early Holocene. Geophysical Research Letters 47(1), e2019GL083164.

Lévesque, Y., St-Onge, G., Lajeunesse, P., Desiage, P. A., Brouard, E., 2020. Defining the maximum extent of the Laurentide Ice Sheet in Home Bay (eastern Arctic Canada) during the Last Glacial episode. Boreas 49(1), 52-70.

Lewis, C. F. M., Todd, B. J., Sonnichsen, G. V., King, T., 2016. Iceberg–seabed interaction on northwestern Makkovik Bank, Labrador Shelf, Canada. In: Dowdeswell, J. A., Canals, M., Jakobsson, M., Todd, B. J., Dowdeswell, E. K., Hogan, K. (Eds.), Atlas of submarine glacial landforms: modern, Quaternary and ancient. Geological Society, London, Memoirs 46, 279-280.

Li, G., Piper, D. J., Calvin Campbell, D., 2011. The Quaternary Lancaster Sound trough-mouth fan, NW Baffin Bay. Journal of Quaternary Science 26(5), 511-522.

1376 Lin, Y., Hibbert, F. D., Whitehouse, P. L., Woodroffe, S. A., Purcell, A., Shennan, I.,
1377 Bradley, S. L., 2021. A reconciled solution of Meltwater Pulse 1A sources using sea-
1378 level fingerprinting. Nature Communications 12, 1-11.

1379 Lindén, M., Möller, P., 2005. Marginal formation of De Geer moraines and their
1380 implications to the dynamics of grounding-line recession. Journal of Quaternary
1381 Science 20(2), 113-133.

1382 Løken, O.H., Hodgson, D.A., 1971. On the Submarine Geomorphology Along the East
1383 Coast of Baffin Island. Canadian Journal of Earth Sciences 8, 185-195.

1384 Lønne, I., 1995. Sedimentary facies and depositional architecture of ice-contact
1385 glaciomarine systems. Sedimentary Geology 98(1-4), 13-43.

1386 Lowry, D. P., Golledge, N. R., Bertler, N. A., Jones, R. S., McKay, R., Stutz, J., 2020.
1387 Geologic controls on ice sheet sensitivity to deglacial climate forcing in the Ross
1388 Embayment, Antarctica. Quaternary Science Advances 1, 100002.

1389 Lysså, A., Vorren, T. O., 1997. Seismic facies and architecture of ice-contact submarine
1390 fans in high-relief fjords, Troms, Northern Norway. Boreas 26(4), 309-328.

1391 MacLean, B., Blasco, S., Bennett, R., Clarke, J. H., Patton, E., 2016. Crag-and-tail
1392 features, Amundsen Gulf, Canadian Arctic Archipelago. In: Dowdeswell, J. A.,
1393 Canals, M., Jakobsson, M., Todd, B. J., Dowdeswell, E. K., Hogan, K. (Eds.), Atlas
1394 of submarine glacial landforms: modern, Quaternary and ancient. Geological
1395 Society, London, Memoirs 46, 53-54.

1396 Margold, M., Stokes, C. R., Clark, C. D., 2018. Reconciling records of ice streaming and
1397 ice margin retreat to produce a palaeogeographic reconstruction of the deglaciation
1398 of the Laurentide Ice Sheet. Quaternary Science Reviews 189, 1-30.

1399 Margreth, A., Gosse, J. C., Dyke, A. S., 2017. Wisconsinan and early Holocene glacial
1400 dynamics of Cumberland Peninsula, Baffin Island, Arctic Canada. Quaternary
1401 Science Reviews 168, 79-100.

1402 Miller, G. H., Andrews, J. T., Short, S. K., 1977. The last interglacial–glacial cycle, Clyde
1403 foreland, Baffin Island, NWT: stratigraphy, biostratigraphy, and chronology.
1404 Canadian Journal of Earth Sciences 14(12), 2824-2857.

1405 Miller, G. H., Wolfe, A. P., Steig, E. J., Sauer, P. E., Kaplan, M. R., Briner, J. P., 2002.
1406 The Goldilocks dilemma: big ice, little ice, or ‘‘just-right’’ ice. Quaternary Science
1407 Reviews 22, 33–48.

1408 Miller, G.H., Wolfe, A.P., Briner, J.P., Sauer, P.E., Nesje, A., 2005. Holocene glaciation
1409 and climate evolution of Baffin Island, Arctic Canada. Quaternary Science Reviews
1410 24, 1703–1721.

1411 Münchow, A., Falkner, K. K., Melling, H., 2015. Baffin island and west Greenland
1412 current systems in northern Baffin bay. Progress in Oceanography 132, 305-317.

1413 Normandeau, A., Dietrich, P., Clarke, J. H., Van Wychen, W., Lajeunesse, P., Burgess,
1414 D., Ghienne, J. F., 2019. The retreat pattern of glaciers controls the occurrence of
1415 turbidity currents on high-latitude fjord deltas.

1416 Ó Cofaigh, C., Dowdeswell, J. A., 2001. Laminated sediments in glacimarine
1417 environments: diagnostic criteria for their interpretation. Quaternary Science
1418 Reviews 20(13), 1411-1436.

1419 Ó Cofaigh, C., Dowdeswell, J. A., Evans, J., Larter, R. D., 2008. Geological constraints
1420 on Antarctic palaeo-ice-stream retreat. Earth Surface Processes and Landforms
1421 33(4), 513-525.

Ó Cofaigh, C., Andrews, J. T., Jennings, A. E., Dowdeswell, J. A., Hogan, K. A., Kilfeather, A. A., Sheldon, C., 2013a. Glacimarine lithofacies, provenance and depositional processes on a West Greenland trough-mouth fan. Journal of Quaternary Science 28(1), 13-26.

Ó Cofaigh, C., Dowdeswell, J. A., Jennings, A. E., Hogan, K. A., Kilfeather, A., Hiemstra, J. F., Noormets, R., Evans, J., McCarthy, D. J., Andrews, J. T., Lloyd, J. M., Moros, M., 2013b. An extensive and dynamic ice sheet on the West Greenland shelf during the last glacial cycle. Geology 41(2), 219-222.

Ó Cofaigh, C., Davies, B. J., Livingstone, S. J., Smith, J. A., Johnson, J. S., Hocking, E. P., Hodgson, D. A., Anderson, J. B., Bentley, M. J., Canal, M., Domack, E., Dowdeswell, J. A., Evans, J., Glasser, N. F., Hillenbrand, C.-D., Larter, R. D., Roberts, S. J., Simms, A. R., 2014. Reconstruction of ice-sheet changes in the Antarctic Peninsula since the Last Glacial Maximum. Quaternary Science Reviews 100, 87-110.

Olsen, I. L., Rydningen, T. A., Forwick, M., Laberg, J. S., Husum, K., 2020. Last glacial ice sheet dynamics offshore NE Greenland – a case study from Store Koldewey Trough. The Cryosphere 14(12), 4475-4494.

Olsen, I. L., Laberg, J. S., Forwick, M., Rydningen, T. A., Husum, K., 2022. Late Weichselian and Holocene behavior of the Greenland Ice Sheet in the Kejser Franz Josef Fjord system, NE Greenland. Quaternary Science Reviews 284, 107504.

Osterman, L. E., Nelson, A. R., 1989. Latest Quaternary and Holocene paleoceanography of the eastern Baffin Island continental shelf, Canada: benthic foraminiferal evidence. Canadian Journal of Earth Sciences 26(11), 2236-2248.

Ottesen, D., Rise, L., Knies, J., Olsen, L., Henriksen, S. 2005. The Vestfjorden-

1446 Trænadjupet palaeo-ice stream drainage system, mid-Norwegian continental shelf.
1447 Marine Geology 218, 175-189.

1448 Ottesen, D., Dowdeswell, J.A., Landvik, J.Y., Mienert, J., 2007. Dynamics of the Late
1449 Weichselian ice sheet on Svalbard inferred from high-resolution sea-floor
1450 morphology. Boreas 36, 286–306.

1451 Ottesen, D., Dowdeswell, J. A., Bellec, V. K., Bjarnadóttir, L. R., 2017. The geomorphic
1452 imprint of glacier surges into open-marine waters: Examples from eastern Svalbard.
1453 Marine Geology 392, 1-29.

1454 Ottesen, D., Batchelor, C. L., Bjarnadóttir, L. R., Wiberg, D. H., Dowdeswell, J. A., 2022.
1455 Glacial landforms reveal dynamic ice-sheet behaviour along the mid-Norwegian
1456 margin during the last glacial-deglacial cycle. Quaternary Science Reviews 285,
1457 107462.

1458 Pendleton, S., Miller, G., Lifton, N., Young, N., 2019. Cryosphere response resolves
1459 conflicting evidence for the timing of peak Holocene warmth on Baffin Island,
1460 Arctic Canada. Quaternary Science Reviews 216, 107-115.

1461 Pieńkowski, A. J., Coulthard, R. D., Furze, M. F., In press. Revised marine reservoir
1462 offset (ΔR) values for molluscs and marine mammals from Arctic North America.
1463 Boreas.

1464 Powell, R. D., 1981. A model for sedimentation by tidewater glaciers. Annals of
1465 Glaciology 2, 129-134.

1466 Powell, R. D., 1990. Glacimarine processes at grounding-line fans and their growth to
1467 ice-contact deltas. In Dowdeswell, J. A., and Scourse, J. D., (Eds), Glacimarine
1468 Environments: Processes and Sediments. Geological Society, London, Special

1469 Publications 53(1), 53-73.

1470 Powell, R.D., Domack, E., 1995. Modern glacio marine environments. In Menzies, J.,
1471 (ed), Glacial Environments: Volume I. Modern Glacial Environments: Processes,
1472 Dynamics and Sediments. Butterworth-Heinemann, Oxford, 445–486.

1473 Powell, R.D., Alley, R.B., 1997. Grounding-line systems: processes, glaciological
1474 inferences and the stratigraphic record. In: Barker, P.F., Cooper, A.C. (Eds.),
1475 Geology and seismic stratigraphy of the Antarctic Margin II. Antarctic Research
1476 Series 71. American Geophysical Union, Washington, 169–187.

1477 Praeg. D.B., MacLean, B. Sonnichsen, G., 2007. Quaternary geology of the Northeast
1478 Baffin Island Continental Shelf, Cape Aston to Buchan Gulf (70° to 72°N).
1479 Geological Survey of Canada, Open File 5409.

1480 Prothro, L. O., Simkins, L. M., Majewski, W., Anderson, J. B., 2018. Glacial retreat
1481 patterns and processes determined from integrated sedimentology and
1482 geomorphology records. Marine Geology 395, 104-119.

1483 Rasmussen, S. O., Bigler, M., Blockley, S. P., Blunier, T., Buchardt, S. L., Clausen, H.
1484 B., Cvijanovic, I., Dahl-Jensen, D., Johnsen, S. J., Fischer, H., Gkinis, V., Guillevic,
1485 M., Hoek, W. Z., Lowe, J. J., Pedro, J. B., Popp, T., Seierstad, I. K., Steffensen, J.
1486 P., Svensson, A. M., Vallelonga, P., Vinther, B. M., Walker, M. J. C., Wheatley, J.
1487 J., Winstrup, M., 2014. A stratigraphic framework for abrupt climatic changes
1488 during the Last Glacial period based on three synchronized Greenland ice-core
1489 records: refining and extending the INTIMATE event stratigraphy. Quaternary
1490 Science Reviews 106, 14-28.

1491 Rydningen, T. A., Vorren, T. O., Laberg, J. S., Kolstad, V., 2013. The marine-based NW
1492 Fennoscandian ice sheet: glacial and deglacial dynamics as reconstructed from

submarine landforms. Quaternary Science Reviews 68, 126-141.

Sheldon, C., Jennings, A., Andrews, J. T., Cofaigh, C. Ó., Hogan, K., Dowdeswell, J. A., Seidenkrantz, M. S., 2016. Ice stream retreat following the LGM and onset of the west Greenland current in Uummannaq Trough, west Greenland. Quaternary Science Reviews 147, 27-46.

Simon, Q., St-Onge, G., Hillaire-Marcel, C., 2012. Late Quaternary chronostratigraphic framework of deep Baffin Bay glaciomarine sediments from high-resolution paleomagnetic data: Geochemistry, Geophysics, Geosystems 13, Q0AO03.

Simon, Q., Hillaire-Marcel, C., St-Onge, G., Andrews, J. T., 2014. North-eastern Laurentide, western Greenland and southern Innuitian ice stream dynamics during the last glacial cycle. Journal of Quaternary Science 29, 14-26.

Slabon, P., Dorschel, B., Jokat, W., Myklebust, R., Hebbeln, D., Gebhardt, C., 2016. Greenland ice sheet retreat history in the northeast Baffin Bay based on high-resolution bathymetry. Quaternary Science Reviews 154, 182-198.

Spagnolo, M., Clark, C. D., Ely, J. C., Stokes, C. R., Anderson, J. B., Andreassen, K., Graham, A. G. C., King, E. C., 2014. Size, shape and spatial arrangement of mega-scale glacial lineations from a large and diverse dataset. Earth Surface Processes and Landforms 39(11), 1432-1448.

Stocker, T. F., Qin, D., Plattner, G. K., Tignor, M., Allen, S. K., Boschung, J., Nauels, A., Xia, Y., Bex, V., Midgley, P. M., (Eds) 2013. Climate change 2013: The physical science basis. Contribution of working group I to the fifth assessment report of the intergovernmental panel on climate change. Cambridge University Press, 1535 pp.

Stokes, C. R., Clark, C. D., 1999. Geomorphological criteria for identifying Pleistocene

ice streams. Annals of glaciology 28, 67-74.

Stokes, C.R., Clark, C.D., 2001. Palaeo-ice streams. Quaternary Science Reviews 20, 1437–1457.

Stokes, C.R., Clark, C.D., 2002. Ice stream shear margin moraines. Earth Surface Processes and Landforms 27, 547–558.

Stokes, C. R., Tarasov, L., Dyke, A. S., 2012. Dynamics of the North American Ice Sheet Complex during its inception and build-up to the Last Glacial Maximum. Quaternary Science Reviews 50, 86-104.

Straneo, F., Hamilton, G. S., Sutherland, D. A., Stearns, L. A., Davidson, F., Hammill, M. O., Stenson, G. B., Rosing-Asvid, A., 2010. Rapid circulation of warm subtropical waters in a major glacial fjord in East Greenland. Nature Geoscience 3(3), 182-186.

Streuff, K., Cofaigh, C. Ó., Noormets, R., Lloyd, J. M., 2017. Submarine landforms and glacimarine sedimentary processes in Lomfjorden, East Spitsbergen. Marine Geology 390, 51-71.

Streuff, K., Cofaigh, C. Ó., Noormets, R., Lloyd, J., 2018. Submarine landform assemblages and sedimentary processes in front of Spitsbergen tidewater glaciers. Marine Geology 402, 209-227.

Syvitski, J. P., 1991. Towards an understanding of sediment deposition on glaciated continental shelves. Continental Shelf Research 11(8-10), 897-937.

Syvitski, J.P.M., Shaw, J., 1995. Sedimentology and geomorphology of fjords, in: Perillo, G.M.E. (Ed.), Developments in Sedimentology. Elsevier, Amsterdam, pp. 113-178.

Syvitski, J., Andrews, J. T., Schafer, C. T., Stravers, J. A., 2022. Sediment fill of Baffin

Island fjords: Architecture and rates. Quaternary Science Reviews 284, 107474.

Tang, C. C., Ross, C. K., Yao, T., Petrie, B., DeTracey, B. M., Dunlap, E., 2004. The circulation, water masses and sea-ice of Baffin Bay. Progress in Oceanography 63(4), 183-228.

Thomas, E.K., Szymanski, J., Briner, J.P., 2010. Holocene alpine glaciation inferred from lacustrine sediments on NE Baffin Island, Arctic Canada. Journal of Quaternary Science 25(2), 146-161.

Tinto, K. J., Padman, L., Siddoway, C. S., Springer, S. R., Fricker, H. A., Das, I., Caratori Tontini, F., Porter, D. F., Frearson, N. P., Howard, S. L., Siegfried, M. R., Mosbeux, C., Becker, M. K., Beretinato, C., Boghosian, A., Brady, N., Burton, N. L. Chu, W., Cordero, S. I., Dhakal, T., Dong, L., Gustafson, C. D., Keeshin, S., Locke, C., Lockett, A., O'Brien, G., Spergel, J. J., Starke, S. E., Tankersley, M., Wearing, M. G., Bell, R. E., 2019. Ross Ice Shelf response to climate driven by the tectonic imprint on seafloor bathymetry. Nature Geoscience 12(6), 441-449.

Trottier, A. P., Lajeunesse, P., Gagnon-Poiré, A., Francus, P., 2020. Morphological signatures of deglaciation and postglacial sedimentary processes in a deep fjord-lake (Grand Lake, Labrador). Earth Surface Processes and Landforms 45(4), 928-947.

Tulaczyk S., Scherer R. P., Clark C. D., 2001. A ploughing model for the origin of weak tills beneath ice streams: a qualitative treatment. Quaternary International 86, 59–70.

Vorren, T. O., Lebesbye, E., Andreassen, K., Larsen, K. B., 1989. Glacigenic sediments on a passive continental margin as exemplified by the Barents Sea. Marine Geology 85(2-4), 251-272.

1562 Weertman, J., 1974. Stability of the junction of an ice sheet and an ice shelf. Journal of
1563 Glaciology 13(67), 3-11.

1564 Winsborrow, M. C., Andreassen, K., Corner, G. D., Laberg, J. S., 2010. Deglaciation of
1565 a marine-based ice sheet: Late Weichselian palaeo-ice dynamics and retreat in the
1566 southern Barents Sea reconstructed from onshore and offshore glacial
1567 geomorphology. Quaternary Science Reviews 29(3), 424-442.

1568 Wise, M. G., Dowdeswell, J. A., Jakobsson, M., Larter, R. D., 2017. Evidence of marine
1569 ice-cliff instability in Pine Island Bay from iceberg-keel plough marks. Nature
1570 550(7677), 506-510.

1571 Woodworth-Lynas, C. M. T., Josenhans, H. W., Barrie, J. V., Lewis, C. F. M., Parrott, D.
1572 R., 1991. The physical processes of seabed disturbance during iceberg grounding
1573 and scouring. Continental Shelf Research 11(8-10), 939-961.

1574 Young, N. E., Briner, J. P., Rood, D. H., Finkel, R. C., 2012. Glacier Extent During the
1575 Younger Dryas and 8.2-ka Event on Baffin Island, Arctic Canada. Science 337,
1576 1330–1333.

1577 Young, N. E., Schaefer, J. M., Briner, J. P., Goehring, B. M., 2013. A ^{10}Be production-
1578 rate calibration for the Arctic. Journal of Quaternary Science 28(5), 515-526.

1579 Young, N. E., Schweinsberg, A. D., Briner, J. P., Schaefer, J. M., 2015. Glacier maxima
1580 in Baffin Bay during the Medieval Warm Period coeval with Norse settlement.
1581 Science Advances 1(11), e1500806.

1582 Young, N. E., Briner, J. P., Miller, G. H., Lesnek, A. J., Crump, S. E., Thomas, E. K.,
1583 Pendleton, S. L., Cuzzone, J., Lamp, J., Zimmerman, S., Caffe, M., Schaefer, J. M.,
1584 2020. Deglaciation of the Greenland and Laurentide ice sheets interrupted by glacier

advance during abrupt coolings. Quaternary Science Reviews 229, 106091.

Young, N. E., Briner, J. P., Miller, G. H., Lesnek, A. J., Crump, S. E., Pendleton, S. L., Schwartz, R., Schaefer, J. M., 2021. Pulsebeat of early Holocene glaciation in Baffin Bay from high-resolution beryllium-10 moraine chronologies. Quaternary Science Reviews 270, 107179.